Responses of runoff to historical and future climate variability over China

Chuanhao Wu[1], Bill X. Hu[1,2*], Guoru Huang[3,4], Peng Wang[1], and Kai Xu[1]

[1] Institute of Groundwater and Earth Sciences, Jinan University, Guangzhou 510632, China.
[2] Department of Earth, Ocean and Atmospheric Sciences, Florida State University, Tallahassee, FL, 32306, USA.
[3] School of Civil Engineering and Transportation, South China University of Technology, Guangzhou 510640, China.
[4] State Key Laboratory of Subtropical Building Science, South China University of Technology, Guangzhou 510640, China.

Correspondence to: Bill X. Hu (bill.x.hu@gmail.com)

Abstract. China has suffered some of the effects of global warming, and one of the potential implications of climate warming is the alteration of the temporal-spatial patterns of water resources. Based on the long-term (1960–2008) water budget data and climate projections from 28 Global Climate Models (GCMs) of the Coupled Model Intercomparison Project Phase 5 (CMIP5), this study investigated the responses of runoff (*R*) to historical and future climate variability in China at both grid and catchment scales using the Budyko-based elasticity method. Results show that there is a large spatial variation in precipitation (*P*) elasticity (from 1.1 to 3.2) and potential evaporation (*PET*) elasticity (from -2.2 to -0.1) across China. The *P* elasticity is larger in northeast and western China than in southern China, while the opposite occurs for *PET* elasticity. The catchment properties elasticity of *R* appears to have a strong non-linear relationship with the mean annual aridity index and tends to be more significant in more arid regions. For the period 1960–2008, the climate contribution to *R* ranges from -2.4 % yr^{-1} to 3.6 % yr^{-1} across China, with the negative contribution in northeast China and the positive contribution in western China and some parts of the southwest. The results of climate projections indicate that although there is large uncertainty involved in the 28 GCMs, most project a consistent change in *P* (or *PET*) in China at the annual scale. For the period 2071–2100, the mean annual *P* is projected to increase in most parts of China, especially the western regions, while the mean annual *PET* is projected to increase in all of China, particularly the southern regions. Furthermore, greater increases are projected for higher emission scenarios. Overall, due to climate change, the arid regions and humid regions of China are projected to become wetter and drier in the period 2071–2100, respectively (relative to the baseline 1971–2000).

Key words: Runoff; Budyko hypothesis; climate elasticity; climate variability; CMIP5 GCMs; China

1 Introduction

Climate change has become increasingly significant (IPCC, 2013), and numerous studies have reported that climate warming is likely leading to the alteration of the hydrological cycle (Oki and Kanae, 2006; Jung et al., 2010). The dynamic properties of the hydrological cycle are governed by the interactions and feedbacks between atmospheric and land surface hydrologic

processes on a catchment scale. The potential consequences of anthropogenic climate change on the hydrological cycle have received significant attention over the last two decades (Wang et al., 2012; IPCC, 2013).

Runoff (*R*), as a commonly adopted indicator of the hydrologic cycle, is critical to human lives and economic activities (Milly et al., 2005). There is a great deal of previous work exploring the impact of climate variations on *R*, with the motivation stemming from the region's vast resources (Christensen et al., 2004; Guo et al., 2009, Piao et al., 2010; Chen et al., 2012; Harding et al., 2012; Wang et al., 2012; Xu et al., 2013b), dangers of flooding (Kay et al., 2006, 2009, 2012; Raff et al., 2009; Liu et al., 2013; Xiao et al., 2013; Wang et al., 2013; Smith et al., 2014; Wu et al., 2014, 2015), and agricultural water uses (Vano et al., 2010). The most common practices in these previous studies are to use the hydrological models driven by the output from Global Climate Models (GCMs) to simulate the hydrological process (e.g., *R*) under future climate change scenarios. However, the key issue faced by such studies is the need to convert coarse resolution GCM outputs to local catchment-scale climatic variables at a higher spatial resolution to serve as the input to a hydrological model (Vano et al., 2015; Wu et al., 2015). The impact assessments are resource intensive and usually subject to uncertainties related to the choice of hydrological model, GCMs, emissions scenarios, and downscaling techniques (Vano et al., 2014, 2015).

With the uncertainty in *R* due to climate change, simple tools able to provide robust estimates of this impact are essential to support policy and planning decisions. Climate elasticity, as an important indicator, provides a measure of sensitivity of the changes in *R* due to the changes in climate. Schaake (1990) made the first attempt to introduce the concept of elasticity and related the climate elasticity of *R* to precipitation (*P*). Since then numerous climate elasticity methods have been developed for evaluating the hydrologic response to climate change all over the world (Schaake, 1990; Dooge et al., 1999; Sankarasubramanian et al., 2001; Milly and Dunne, 2002; Fu et al., 2007; Zheng et al., 2009; Ma et al., 2010; Yang and Yang, 2011; Yang et al., 2014; Vano et al., 2015). Sankarasubramanian et al. (2001) provided a detailed category of climate elasticity methods for modelling climate change impacts. One of the most common methods is to analytically derive the sensitivity of *R* based on the Budyko hypothesis, due to its clear theory and that it does not rely on a large amount of data (Yang and Yang, 2011). More importantly, the Budyko-based elasticity method can derive the climate elasticity and can also represent the impact of the catchment characteristics through the parameters of the Budyko model. Accordingly, it is widely applied for the assessment of the hydrologic impacts of climate change (Dooge et al., 1999; Zheng et al., 2009; Yang and Yang, 2011; Yang et al., 2014).

China is a vast land, spanning many degrees of latitude with complicated terrain, which results in a large regional variation in climate elasticity. The investigation of the *P* elasticity of *R* has been reported in many regions of China, such as the Miyun

Reservoir basin (Ma et al., 2010), Luan River basin (Xu et al., 2013a), the headwater catchments of the Yellow River basin (Zheng et al., 2009), Poyang Lake basin (Sun et al., 2013), and Hai River and Yellow River basins (Yang and Yang, 2011; Liu and McVicar, 2012). Recently Yang et al. (2014) investigated the climate elasticity of *R* for the 210 catchments of China based on the Budyko-based elasticity approach. The results indicated that the *P* elasticity exhibits a large regional variation, with a small range in southern China, the Songhua River basin and the northwest and a large range in the Hai River basin, the Yellow River basin, and the Liao River basin. Although the aforementioned studies have certainly made advances in understanding the climate elasticity of *R* in China, our knowledge about the responses of *R* to climate change over various temporal and spatial scales remains rather limited due to the large regional variation in climate types and catchment characteristics. The question of how climate change will affect *R* over China in the future is also an important problem to be addressed. Developing a more accurate and quantitative understanding of the changing water resources over various temporal and spatial scales under a changing environment is therefore a high priority for China.

Based on the unique long-term (1960–2008) land surface dataset of China and the climate projections from 28 GCMs of the Coupled Model Intercomparison Project Phase 5 (CMIP5), the objectives of this research are (1) to investigate the changes of *R* and climate variables and their relationship at an interannual scale; (2) to estimate quantitatively the climate elasticity and catchment properties elasticity of *R* across China at both grid and catchment scales; and (3) to predict climate change and the changes in *R* due to future climate change for China from the CMIP5 projections at both grid and catchment scales.

2 Data and methodology

2.1 Data sets

Monthly data of potential evaporation (*PET*) covering the period 1960–2008 over China are provided by the Hydroclimatology Group of Princeton University (Sheffield et al., 2006, 2012). The *PET* is estimated by the Penman equation (Penman, 1948; Shuttleworth, 1993), using the updated meteorological dataset obtained from Sheffield et al. (2006, 2012). A long-term (1960–2008) daily land surface dataset over China, including *P*, surface runoff (*RS*), and baseflow (*BS*), with a 0.25 degree spatial resolution were obtained from the Land Surface Processes and Global Change Research Group (Zhang et al., 2014). In this dataset, *P* is driven by interpolating gauged daily precipitation from 756 meteorological stations of the Chinese Meteorological Administration (CMA). *RS* and *BS* are derived from the Variable Infiltration Capacity (VIC) model forced by the gridded daily climate forcings (i.e. *P*, maximum and minimum temperature, and wind speed). VIC model parameters, including the infiltration shape parameter, the second and third soil layer depths, and the three parameters in the base flow scheme, were estimated by using an optimization algorithm of the multi-objective complex evolution of the University of Arizona (Zhang et al., 2014). The simulated monthly *RS* and *BS* match well with the observations at the large

river basins in China (Zhang et al., 2014). Compared with the global product of a similar nature, this dataset provides a more reliable estimate of land surface variables over China (Nijssen et al., 2001; Adamet al., 2006; Rodell et al., 2004; Sheffield et al., 2006; Sheffield and Wood, 2007; Pan et al., 2012). In this study, the data of *P*, *RS*, and *BS* are initially regridded onto 0.5° grids over China using the linear interpolation method. All the daily data (*P*, *RS*, and *BS*) and monthly data (*PET*) are then aggregated temporally for the annual scale over China. The *R* was calculated by the sum of *RS* and *BS* at each of the 0.5° grid points.

Climate projections from 28 CMIP5 GCMs (as shown in Table 1) are provided by the Canadian Climate Data and Scenarios (CCDS, http://www.cccsn.ec.gc.ca/index.php?page=gridded-data). These data, including simulations of surface air temperature (*T*), *P*, sea ice thickness, sea ice concentration, snow depth, and near-surface wind speed, are statistically downscaled and regridded onto a common 1°×1° global grid by the CCDS. In this study, monthly *P* and monthly *T* over China, including one historical simulation for the period 1971–2000 and three emission scenarios (RCP2.6, RCP4.5, and RCP8.5) for the future period 2071–2100 from each of the 28 CMIP5 models and the multi-model ensemble of 28 CMIP5 models, are used for the projections of climate change. The data are initially disaggregated to 0.5° grids over China then corrected by using a 'delta change' method (Wu et al., 2016), on the basis of the observed data of *P* and *T* as provided by the Climatic Research Unit (CRU) of the University of East Anglia (Harris et al., 2014).

Figure 2 shows the comparison of observed mean annual *T* and *P* and the corresponding simulations from 28 CMIP5 models before and after bias correction for the 14 basins in China. The basin number is consistent with that given in Figure 1. As shown, the uncorrected model simulations tend to underestimate *T* and overestimate *P* for most of the basins, with more uncertainties for the simulation of *P* than for *T*. Compared to the uncorrected model results, the bias correction results represent large improvements and show a good agreement with the observed values for these basins. Therefore, the bias correction model simulations are acceptable for the investigation of climate change projections in this study.

From the GCM data, the *PET* for the periods 1971–2000 and 2071–2100 under different emission scenarios are initially estimated by the Thornthwaite method (Thornthwaite, 1948) and then corrected by a multiplicative bias correction method as follows:

$$PET_{cor,GCM,i} = PET_{Th,GCM,i} \times \frac{\overline{PET}_{Pen,obs,i}}{\overline{PET}_{Th,obs,i}} \quad (1)$$

where $PET_{cor,GCM,i}$ and $PET_{Th,GCM,i}$ are bias-corrected annual *PET* and the *PET* calculated from the Thornthwaite method, respectively, for the *i*th grid point of the GCMs. $\overline{PET}_{Pen,obs,i}$ and $\overline{PET}_{Th,obs,i}$ are the 49-year (1960–2008) averages of

123 *PET* calculated from the Penman and Thornthwaite methods, respectively, for the *i*th grid point.

124

125 Based on the *T* data from the CRU, the Thornthwaite method is used to calculate *PET* to test the applicability of Equation (1).
126 Figure 3 shows a comparison of annual *PET* calculated from the Penman method and that from the Thornthwaite method
127 corrected by Equation (1) during the period 1960–2008. It is clear that the corrected *PET* agrees well with the *PET* from the
128 Penman method, with the correlation coefficients of 0.94 and 0.958 at the catchment and grid scales, respectively. This
129 suggests that Equation (1) can be acceptable for the bias correction of *PET* in the GCMs.

130

131 **2.2 Sensitivity of runoff to climate and catchment properties**

132 The Budyko framework has been widely used to study basin-scale water and energy balances. Two of the one-parameter
133 formulations of the Budyko curve proposed by Choudhury (1999) (Equation (2), see also Yang et al., 2008) and Fu (1981)
134 (Equation (3), see also Zhang et al., 2004) are expressed as:

135 $$E = P\frac{PET}{(P^n + PET^n)^{1/n}}, \quad n \in (0,\infty) \tag{2}$$

136 $$E = P + PET - (P^\omega + PET^\omega)^{1/\omega}, \ \omega \in (1,\infty) \tag{3}$$

137 where n and ω are empirical parameters, representing the effects of other factors (e.g. land surface characteristics, the
138 average slope, vegetation type or land use, and climate seasonality) on the water-energy balance (Yang et al., 2008, 2014;
139 Roderick and Farquhar, 2011; Li et al., 2013a). Yang et al. (2008) calibrated the parameters n and ω using long-term water
140 balance data from 108 catchments from the nonhumid regions of China and found that these two empirical parameters are
141 linearly correlated.

142

143 Based on the Budyko hypothesis and assuming steady state conditions, Roderick et al. (2011) and Yang and Yang (2011)
144 derived the elasticity method to estimate the contribution to *R* from the changes in climate (represented by *P* and *PET*) and
145 catchment properties as follows:

146 $$\frac{dR}{R} = \varepsilon_P \cdot \frac{dP}{P} + \varepsilon_{PET} \cdot \frac{dPET}{PET} + \varepsilon_n \cdot \frac{dn}{n} \tag{4}$$

147 where $\varepsilon_P, \varepsilon_{PET}$, and ε_n represent the elasticity coefficients of *P*, *PET*, and catchment properties respectively, and are
148 expressed as:

149 $$\varepsilon_P = \frac{P}{R}\left(1 - \frac{\partial E}{\partial P}\right) \tag{5a}$$

$$\varepsilon_{PET} = -\frac{PET}{R}\frac{\partial E}{\partial PET} \quad (5b)$$

$$\varepsilon_{n} = -\frac{n}{R}\frac{\partial E}{\partial n} \quad (5c)$$

where $\frac{\partial E}{\partial P}, \frac{\partial E}{\partial PET}$, and $\frac{\partial E}{\partial n}$ denote the first order partial derivatives of the Budyko equation with respect to *P*, *PET*, and the parameter *n*. In this study, both Equations (2) and (3) are used for the estimation of the elasticity of *P*, *PET*, and catchment properties over China.

2.3 Trend estimate method

The Mann-Kendall (M-K) nonparametric test (Mann, 1945; Kendall, 1975) is an effective tool for detecting the statistical significance of trends in the time series of meteorological and hydrological variables (Yang et al., 2014; Wu and Huang, 2015). In this study, the M-K method is used to detect the significance of monotonic trends in hydroclimatic time series. The nonparametric trend slope estimator developed by Sen (1968) is used for the magnitude estimation of the trends in a hydroclimatic time series.

3 Results

3.1 Interannual variability of climatic variables and runoff

The standard deviations for annual *P*, *PET*, and *R* are computed for each of the 0.5° grids in China, and the *PET* deviation ratio (σ_{PET}/σ_P) and the *R* deviation ratio (σ_R/σ_P) are calculated. The spatial distributions of *PET* deviation ratio and *R* deviation ratio across China are displayed in Figure 4(a) and (b). As shown, the *PET* deviation ratio is rather small in most parts of China, especially the southern regions, while a larger value is observed mainly in the Xinjiang region, where there are greater aridity indices. Generally, atmospheric water is enough to accommodate the limited *PET* in humid climates, which would lead to a limited response of *PET* to *P* variability. Specifically, the interannual variability of *PET* is more sensitive to that of *P* in arid climates (with water limits) than in humid climates (with energy limits). In contrast to the *PET* deviation ratio, the *R* deviation ratio tends to increase from arid climates to humid climates. The reason for this is that, in arid climates, the catchment water supply is very limited and gives priority to evaporation and soil storage capability, which leads to little variation in *R*.

Figure 4(c) shows the relationship between the *R* deviation ratio and mean annual aridity index ($\bar{\phi}$) for all 0.5° grids in China. As indicated, $\bar{\phi}$ is a major control for the *R* deviation ratio under not very dry conditions (e.g. $\bar{\phi}$ <10); that is, the *R*

deviation ratio decreases with increased $\overline{\phi}$. However, under very dry conditions (e.g. $\overline{\phi}$>10) the *R* deviation ratio becomes insensitive to $\overline{\phi}$, since in this case, other factors, such as soil storage capacity, can also have a large impact on the variation of *R*.

3.2 Sensitivity of runoff to climate and catchment properties

3.2.1 Climate elasticity

The *P* elasticity and *PET* elasticity of *R* based on Equations (2) and (3) are estimated at each of the 0.5° grids in China. As shown in Figure 5, the spatial patterns of *P* elasticity and *PET* elasticity from Equations (2) and (3) are almost the same in all regions of China. There is a large spatial variation in *P* elasticity and *PET* elasticity, i.e. ranging from 1.1 to 3.2 and from -2.2 to -0.1 across China, respectively. In particular, *P* elasticity is more significant in the northeast and western areas than in southern China, which is in contrast to *PET* elasticity. Figure 6 shows the relationship between $\overline{\phi}$ and climate (*P* and *PET*) elasticity. As shown, the *P* (*PET*) elasticity first increases (decreases) and then decreases (increases) with the increase of $\overline{\phi}$ under not very dry conditions (i.e. $\overline{\phi}$<10). However, when $\overline{\phi}$ becomes large enough (e.g. $\overline{\phi}$>10), both *P* and *PET* elasticity becomes insensitive to $\overline{\phi}$.

The climate elasticity estimated for each of the 14 large basins is shown in Table 2. The values of *P* elasticity are in the range of 1.39–2.28, with a larger (~smaller) elasticity in the Haihe River and Inner Mongolia River (Southwest Drainage). A similar phenomenon is found for *PET* elasticity, which suggests that Haihe River (Southwest Drainage) is the most (least) sensitive to *PET* among the 14 basins. Overall the values of *P* elasticity and *PET* elasticity derived by Equation (2) are very close to those from Equation (3), but the difference between them tends to be larger for dry basins with increasing aridity indices.

By using the estimates of climate elasticity derived by Equation (2), the change in *R* as a function of the percentage change in *P* and *PET* is calculated for the 14 basins (Figure 7). The *R* is positively related to *P* and negatively related to *PET*, and the magnitudes and patterns of the response of *R* to changes in *P* and *PET* vary in different scales. Generally, the *R* is more sensitive to climate in the Haihe River and Inner Mongolia River, while relatively weak sensitivity is found in the Southwest Drainage and Yangtze.

3.2.2 Catchment properties elasticity

The spatial distributions of catchment properties elasticity from Equations (2) and (3) are displayed in Figure 5(e) and (f). As shown, the catchment properties elasticities for these two equations are rather similar across China, and the values of Equation (3) are generally smaller than those from Equation (2). Regarding the spatial pattern, the catchment properties elasticity is very weak (approximately equal to 0) in southern China and some regions of northeast China, but it tends to be more significant in some water-limited regions of northwest China. Figure 6(c) shows the relationship between $\overline{\phi}$ and the parameter elasticity for all 0.5° grids in China. It suggests that $\overline{\phi}$ is a major control for catchment properties elasticity across China, i.e. the catchment properties elasticity would become stronger with increasing aridity indices. The catchment properties elasticities estimated for the 14 large basins are shown in Table 2. The catchment properties elasticity shows a large spatial variation, ranging from -2.78 to -0.24 for Equation (2) and from -4.3 to -0.33 for Equation (3). Overall, the changes in *R* are more sensitive to catchment properties in arid basins with larger aridity indices, which is consistent with the findings at the grid scale.

3.3 Climate change during 1960–2008

The annual trend magnitudes in *P*, *R*, *PET*, and aridity index during the period 1960–2008 are shown in Figure 8 (a), (b), (c), and (d). As indicated, both *P* and *R* show an increasing trend mainly in the northwest and southeast regions and a decreasing trend mainly in the central region and North China plain. A significant increasing in *PET* is detected mainly in northeast China and eastern China, while the decreases mainly occur in most parts of western China. The aridity index tends to show an increasing trend in most parts of China, indicating an increasing risk of meteorological drought in these regions during the past several decades. In contrast, the decrease of aridity index is only found in some parts of western China.

3.4 Changes in runoff due to climate change during 1960–2008

Using the estimates of climate elasticity from Equation (2), the contributions of *P*, *PET*, and climate (i.e. *P*& *PET*) to *R* in China for the period 1960–2008 are calculated (as shown in Figure 8(e), (f), and (g)). A positive contribution (up to 3.7 % yr^{-1}) from *P* to *R* is mainly recorded in western China, while a negative contribution is found mainly in northeast China and North China plain. Negative and positive contributions of *PET* to *R* mainly occur in northeast China and western China, respectively. The contributions of climate, i.e. the sum of the contributions from *P* and *PET*, ranges from -2.4 % yr^{-1} to 3.6 % yr^{-1} across China. The spatial pattern of climate is rather similar to that of *P*, showing a negative contribution in northeast China and a positive contribution in western China and some parts of the southeast. Particularly, the largest positive contribution of climate occurs in the Tibetan plateau. The contributions of *P*, *PET*, and climate (i.e. *P*& *PET*) to *R* in the 14 river basins for the period 1960–2008 are shown in Table 3. A positive contribution of *P* is detected in Southeast Drainage, Southwest Drainage, Qiangtang, Qinghai, Xinjiang and Hexi, while an oppoiste contribution is found in other basins. In

contrast, a negative contribution of *PET* is found in most of the basins (except for Qiangtang and Hexi). In general, there is an increased *R* in Southeast Drainage, Southwest Drainage, Qiangtang, Qinghai, Xinjiang and Hexi (from 0.06 to 1 % yr^{-1}) and a decreased *R* in other basins (from -1.12 to -0.12 % yr^{-1}).

3.5 Future climate change

Figure 9 shows the uncertainty range of the relative change in mean annual *P* and *PET* in the basins for the period 2071–2100 under the RCP2.6, RCP4.5, and RCP8.5 scenarios as predicted by 28 CMIP5 models (relative to the baseline 1971–2000). As shown, there is a large difference between different GCMs and emission scenarios, which highlights the uncertainty inherent in projections of climate change. However, overall *P* is projected to increase in most of the basins, and greater increases are projected for higher emission scenarios. Meanwhile, greater increases tend to be projected for more arid basins, suggesting a decreasing risk of meteorological drought in the future. The average changes (red dotted lines) of mean annual *P* for the 14 basins range from 2.4 % to 11.0 % in RCP2.6, from 4.2 % to 16.0 % in RCP4.5, and from 3.1 % to 23.7 % in RCP8.5. The largest increase in the RCP2.6 and RCP8.5 scenarios is found for the Qinghai River, while the largest increase in the RCP4.5 scenario is projected for the Hexi River. For *PET*, there is an increase projected in all basins due to climate warming, with the largest and smallest increases in the RCP8.5 and RCP2.6 scenarios, respectively. However, a large uncertainty exists among the GCMs, which is similar to that for *P*. Furthermore, the uncertainty range tends to be larger with higher emission scenarios. The average changes (red dotted lines) of *PET* for the basins range from 7.0 % to 12.0 % in RCP2.6, from 13.5 % to 22.2 % in RCP4.5, and from 27.9 % to 49.8 % in RCP8.5. The largest and smallest average increases are projected for the Pearl River and Qiangtang River, respectively.

Figure 10 displays the multi-model ensemble median relative change in mean annual *P* and *PET* in China for the period 2071–2100 (relative to the baseline 1971–2000). The projected changes in *P* (or *PET*) have a similar spatial pattern for the three emission scenarios; that is, *P* is projected to show an increase in western China and the northeast, and *PET* is projected to increase significantly in southern China and some parts of the Tibetan plateau, especially for the RCP8.5 scenario. In addition, note that there are small changes in *P* and significant increases in *PET* projected for southern China. This would result in an increasing risk of meteorological drought in the future.

3.6 Future changes in runoff due to climate change

Based on the estimates of elasticity from Equation (2), the percentage changes in the contributions of annual *P* and *PET*, as well as climate, to *R* from the 28 GCMs for the period 2071–2100 are calculated for each of the 14 basins (relative to the baseline 1971–2000). As shown in Figure 11, the changes in *P* contribution mainly follow the changes in *P* (Figure 9). A

positive contribution from *P* is projected for most of the basins, and larger contributions occur in more arid basins, as well as in higher emission scenarios. Negative contributions of *PET* to *R* are projected for all basins due to the negative coefficients of *PET* elasticity. Smaller contributions of *PET* are mainly found in the Southwest Drainage. In contrast, larger contributions are projected mainly in the Huaihe River, Haihe River, and Inner Mongolia River, where the percentage decreases from the 28 models can be up to 25 %, 35 %, and 90 % in the RCP2.6, RCP4.5 and RCP8.5 scenarios, respectively.

Climate change is projected to reduce the *R* in some humid basins, such as the Southeast Drainage and Pearl River, where the average changes in the three emission scenarios range from -22.83 % to -3.0 % and from -23.6 % to -3.5 %, respectively (Figure 11 (g), (h) and (i)). For other basins, particularly for arid basins, the *R* is projected to increase due to climate change. The largest average changes in *R* under the RCP2.6 and RCP4.5 scenarios are found in the Qinghai River (12.85 % and 16.18 %, respectively). For the RCP8.5 scenario, they are found in the Qiangtang River (18.59 %). Note that there is an obvious decrease in *R* (-17.59 %) projected for the Huaihe River under RCP8.5 scenario, which is mainly caused by the larger negative contribution of *PET*.

Figure 12 shows the spatial distributions of the relative changes in the contributions of annual *P* and *PET* as well as climate to *R* in China for 2071–2100. This is based on the CMIP5 multi-model ensemble medians. Compared with the baseline 1971–2000, the increases in *R* due to the changes in *P* are projected in western China and some parts of northern China, and this phenomenon is particularly significant in the RCP8.5 scenario (up to 60.3 %). In contrast, the changes in *PET* are projected to reduce the *R* in all of China, with the larger decreases occurring mainly in the North China plain, northeast, and some parts of western China. Overall, climate change is projected to cause an obvious increase (decrease) of *R* in western China (southern China) under any emission scenario (Figure 12(g), (h) and (i)). This suggests that the arid regions (humid regions) in China will become wetter (drier) in the future.

4 Discussion

4.1 The estimation of elasticity

The Budyko-based elasticity method is applied to quantify sensitivity of runoff to climate and catchment properties across China. Two Budyko models proposed by Choudhury (1999) and Fu (1981) are used for the comparison of the estimation of the climate elasticity of *R*. The results suggest that the climate elasticity is insensitive to the Budyko equations. The climate elasticity of *R* has been estimated in many regions of China. For example, the values of *P* elasticity are estimated as 2.4 for the Miyun Reservoir basin (Ma et al., 2010), 2.6 for the Luan River basin (Xu et al., 2013a), 2.1 for the headwater catchments of the Yellow River basin (Zheng et al., 2009), 1.4–1.7 for the Poyang Lake basin (Sun et al., 2013), 1.7–3.1 for

the Hai River basin (Xu et al., 2014), 1.1–2.0 for southern China, the Songhua River basin, and the northwest, 2.1–4.8 for the Hai River basin, the Yellow River basin, and the Liao River basin (Yang et al., 2014), and 1.6–3.8 for the 63 catchments of China (Yang and Yang, 2011). In addition, the *PET* elasticity is estimated as -1.04 for the headwater catchments of the Yellow River basin (Zheng et al., 2009) and from -1 to -0.2 for the Poyang Lake basin (Sun et al., 2013). Those results are close to our results for *P* elasticity ranging from 1.1 to 3.2, and for *PET* elasticity ranging from -2.2 to -0.1 in China. It is worth noting that the values of *P* elasticity tend to be larger in the northeast and some parts of western China that are located in arid climates. This is in good agreement with the findings by Sankarasubramanian et al. (2001), which indicated that a larger *P* elasticity occurs in more arid regions. However, some parts of Xinjiang, which is more arid than southern China, have smaller *P* elasticity. Meanwhile, some parts of southern China, which is more humid than other regions in China, have larger *P* elasticity (Figure 5). In addition, the Haihe River basin, located in less arid climates than that of the northwest, shows the largest *P* elasticity in China (Table 2). A similar phenomenon is also introduced in Yang et al. (2014). One of the major reasons for this difference may be attributed to the impacts of human activities that alter the patterns of *R* in these regions. In addition, uncertainties in water budget data, such as the errors in the simulation of *R* and in the estimation of *PET*, may also contribute to this difference.

The comparisons for the estimates of ε_n and ε_ω suggest that although the values of ε_n and ε_ω are mainly dependent on the parameters of Budyko models, the spatial pattern of ε_n is consistent with that of ε_ω at the 0.5^o grid points over China (Figure 5(e) and (f)). Yang et al. (2008) indicated that the parameters n and ω from Equations (2) and (3) are linearly correlated. We also conducted a regression analysis of ε_n and ε_ω for all 0.5^o grid points over China and found a strong linear correlation between ε_n and ε_ω ($\varepsilon_\omega = 1.7061\varepsilon_n + 0.0986$, $r^2 = 0.96$). In addition, our results show that *R* is more sensitive to catchment properties (ε_n and ε_ω) in the more arid regions (Figure 5(e) and (f)). The possible internal connection is that the arid regions with less vegetation coverage and stronger evaporation do not effectively hold the rainfall water that will be evaporated, leading to the smaller proportion of rainfall for *R*.

4.2 Sensitivity analysis for *PET* calculation methods

We compare four *PET* calculation methods, including the Penman method, the Thornthwaite method, the FAO-56 Penman–Monteith method (Allen et al., 1998), and the Thornthwaite method corrected by Equation (1), to test the robustness of the *PET* elasticity result subject to *PET* uncertainties. In terms of mean annual *PET* as shown in Figure 13 (a), the Thornthwaite method gives relatively low *PET* among the four methods, especially in arid basins (e.g., Qiangtang, Qinghai, Xinjiang and Hexi). This is in agreement with previous studies, which indicated that the Thornthwaite method tends to underestimate *PET* in the arid areas (Hashemi and Habibian, 1979; Malek 1987; Garcia et al., 2004). In contrast, the mean annual *PET* by the

other three methods are quite consistent, especially for the Penman method and the Thornthwaite method corrected by Equation (1). A similar result was also reported by Zeng and Cai (2016), which indicated that estimations of water balance at both annual and month scales are generally robust under various *PET* calculation methods (not including the Thornthwaite method). The *PET* elasticity calculations from the four different *PET* data for the 14 river basins are shown in Figure 13(b). The Thornthwaite method yields stronger *PET* elasticity than other three methods in most of the basins mainly due to the underestimation of *PET*. However, the other three methods give very similar results in all 14 basins. In summary, the estimation of *PET* elasticity is robust to the *PET* calculations from the Penman method, the FAO-56 Penman–Monteith method, and the Thornthwaite method corrected by Equation (1), but is not acceptable for the Thornthwaite method.

In general, the Thornthwaite method corrected by Equation (1) significantly improves the accuracy of *PET* (Figure 3 and Figure 13(a)). However, it should be emphasized that the Thornthwaite method is an empirical equation that neglects the effects of atmospheric conditions, such as wind speed, humidity and radiation (McVicar et al., 2012). In addition, the Equation (1) used for the bias correction of *PET* belongs to a 'delta method' (Graham et al., 2007; Sperna Weiland et al., 2010), which only considers the average change but ignores the differences in the standard deviation and the coefficient of variation between the projection and baseline periods (Watanabe et al., 2012). Therefore, a more physically-based *PET* calculation method (such as the Penman method) needs to be considered in the GCMs to fully understand the *PET* calculation uncertainties in the projections of climate change.

4.3 The projections of climate change and runoff

The hydrological impacts of climate change have been investigated in many regions of China, such as the Hanjiang basin (Chen et al., 2007; Guo et al., 2009), the catchment of the Loess Plateau (Wang et al., 2013), the Qingjiang River basin (Chen et al., 2012), the Qiantang River basin (Xu et al., 2013b), the Songhuajiang River basin (Su et al., 2015), the southeastern Tibetan Plateau (Li et al., 2013b), the Pearl River basin (Yan et al., 2015), the Xin River basin (Zhang et al., 2016), the sub-catchments of the Yangtze and Yellow River basins (Xu et al., 2011), the Huang-Huai-Hai region (Lu et al., 2012), and ten major river basins in China (Wang et al., 2012). There is a large uncertainty involved in these impact studies, which results in a large difference in climate projections. For example, Wang et al. (2012) indicated that the prevailing pattern of "north dry and south wet" in China will likely be exacerbated under future climate warming. However, the results of most GCMs in this study suggest that the arid regions and humid regions of China are projected to become wetter and drier in the future, respectively. The main difference between the two studies is the use of different climate models, emission scenarios, and time periods. This also demonstrates that the results of climate projections should be taken with caution, since the regional climate simulations (especially of precipitation) from the GCMs are still not robust at the present stage.

This study focuses on the hydrological change due to climate change (i.e., changes in *P* and *PET*), while the effects of the variability of catchment properties (e.g., land cover change, groundwater and river water extraction, urbanization, irrigation, etc.) on the hydrology are overlooked here. Most of the available GCMs lack of key regional feedback processes involving land use, such as forest plantations, irrigation, and urbanization feedbacks that are critically important throughout China (Piao et al., 2010). The projected changes in catchment properties therefore need to be involved in the GCMs to account for their hydrological impacts. In addition, recent studies indicated that plant responses to increasing CO_2 tend to keep more water on land, therefore resulting in a greater increase in *R* (Milly and Dunne, 2016; Swann et al, 2016). That is to say, the hydrological models (e.g., VIC model), without the schemes of the plant stomatal responses to CO_2, would lead to an underestimation of *R* under high CO_2. Therefore, the implications of plants needing less water under high CO_2 should be included in the assessment of hydrological impacts of climate change.

4.4 Uncertainties

Generally, a multitude of sources of uncertainty are involved in the impact assessment of climate change. In this study, uncertainty mainly comes from the GCMs, emission scenarios, the elasticity method, and the estimation error of the water budget data. To highlight the uncertainty from the GCMs, the 28 GCMs as produced by different research institutes around the world, are used for the comparison of climate change projections. There exists a large difference in the projections of *P* and *PET* among the 28 GCMs. Particularly, the uncertainty range of *P* tends to be larger for more arid regions, while the uncertainty range of *PET* tends to be larger for more humid regions (Figure 9). This highlights the impact of potential misleading conclusions if only one climate model were to be used for the impact assessments. The large uncertainty driven by the GCMs in relation to the hydrological impacts of climate change has been reported in many previous studies (Kay et al., 2009; Prudhomme and Davies, 2009; Chen et al., 2011; Teng et al., 2012; Liu et al., 2013; Wu et al., 2014, 2015). It is worth noting that although the projected ranges of *P* and *PET* show large variability in various GCMs, most project a consistent change (i.e. increase) in *P* and *PET* for the future period (Figure 9). In contrast, the uncertainty from the emission scenarios is smaller than that from the GCMs, since the projected changes in *P* (or *PET*) show a similar pattern under all emission scenarios (Figure 9). The main difference is that the projected changes tend to be more significant in higher emission scenarios.

The elasticity equation (i.e. Equation (4)) used in this study is driven from the linear approximation of the Budyko equation (Equations (2) and (3)) by neglecting the higher order. Such approximation would possibly lead to an uncertainty in the estimation of climate elasticity. Yang et al. (2014) indicated that the error in estimation of elasticity tends to increase with

increasing changes in *P* and *PET*, as well as the increased parameter of the Budyko equation. Future research is needed to quantify the effects of the errors on the estimation of elasticity under various climate conditions.

In addition to uncertainty in *PET* calculation (as discussed in section 4.2), there are also uncertainties associated with the estimates of other water budget components, such as *R*. As shown in Figure 14, the sensitivity of climate (i.e., *P* and *PET*) elasticity to *R* varies considerably between basins and tends to be larger in more humid basins. Moreover, *PET* elasticity is more sensitive to changes in *R* compared with *P* elasticity for all 14 basins. As indicated by Zhang et al. (2014), although the *R* is realistically estimated for most of the basins (especially for humid basins) in China with a small relative error, there is still a large relative error for few arid basins in western China due to the lack of meteorological observations. Therefore, the large errors in simulated *R* of the VIC model may result in large uncertainties in elasticity calculation, particularly in western China. Also note that some other natural water sources, such as snow and glaciers, which may contribute to *R*, are overlooked in this study. Lute and Abatzoglou (2014) highlighted the importance of extreme snowfall events in shaping the interannual variability of the water balance. The melting of snow and glaciers is generally significant at a seasonal time scale in some high altitude regions of China. Neglecting the effects of snow and glaciers would lead to a bias in the modelling of *R* for these regions.

5 Conclusion

In this study, the Budyko-based elasticity method was used to investigate the responses of runoff to historical and future climate variability over China at both grid and catchment scales. The climate and catchment properties elasticities of runoff were estimated based on the long-term (1960–2008) land surface data from Zhang et al. (2014). Twenty-eight GCMs with three emission scenarios from the CMIP5 were collected for the projections of climate change and its contribution to runoff in China during the period 2071–2100. The uncertainties associated with the estimates of *PET*, *R*, climate elasticity, as well as climate projections, are discussed in detail. The main findings are summarised as follows:

(1) The interannual variability of *PET* is more sensitive to that of *P* in more arid regions, while the opposite occurs in the response of interannual variability of *R* to that of *P*. A large spatial variation exists in *P* elasticity (from 1.1 to 3.2) and *PET* elasticity (from -2.2 to -0.1) across China. The *P* elasticity is larger in northeast and western China than in southern China, which is opposite to that of *PET* elasticity. Among the 14 river basins, the Haihe River and Southwest Drainage have the largest and smallest climate elasticities, respectively. The catchment properties elasticity of *R* is sensitive to mean annual aridity indices and tends to be stronger in more arid regions with increasing aridity indices.

(2) For the period 1960–2008, the positive (negative) contributions from *P* to *R* are mainly found in western China (northeast China and North China plain), and the positive (negative) contributions of *PET* mainly occur in western China (northeast China). Overall, the climate contribution to *R* ranges from -2.4 % yr^{-1} to 3.6 % yr^{-1} across China during the period 1960–2008, with a negative contribution in northeast China and a positive contribution in western China and some parts of the southwest. The largest positive and negative contributions of climate occur in the Qiangtang and Haihe River basins, respectively.

(3) There is a large uncertainty in climate projections among the 28 GCMs. Moreover, the uncertainty range of the *P* (*PET)* projection tends to be larger for more arid (humid) regions. However, most of the GCMs project a consistent change in annual *P* or annual *PET*. For the period 2071–2100, the *P* is projected to increase in most parts of China, especially the western regions, and the *PET* is projected to increase in all of China, particularly the southern regions. Furthermore, greater increases are projected for higher emission scenarios. Due to future climate warming, the arid regions and humid regions of China are projected to become wetter and drier in the period 2071–2100, respectively (relative to the baseline 1971–2000).

The results of this study (especially of the climate change projections) should be taken with caution, since uncertainties in the results exist because of several issues, including the different simulations of GCMs, the estimation error of climate elasticity, and the estimation error in the water budget components. A thorough investigation of the uncertainty involved in the hydrologic effects of climate change in China should be considered in future research.

Acknowledgements

This research was supported by the Fundamental Research Funds for the Central Universities (Grant No. 21617301) and partly supported by funding from the National Natural Science Foundation of China (Grant No. 41530316) and the National Key Research and Development Program of China (Grant No. 2016YFC0402805).

References

Adam, J. C., Clark, E. A., Lettenmaier, D. P., and Wood, E. F.: Correction of global precipitation products for orographic effects, J. Climate., 19, 15–38, 2006.

Allen, R., Pereira, L., Raes, D., and Smith, M.: Crop evapotranspiration - Guidelines for computing crop water requirements, FAO, Rome, 1998.

Chen, H., Guo, S. L., Xu, C. Y., and Singh, V. P.: Historical temporal trends of hydro-climatic variables and runoff response to climate variability and their relevance in water resource management in the Hanjiang basin, J. Hydrol., 344, 171–184,

455 doi:10.1016/j.jhydrol.2007.06.034, 2007.
456 Chen, H., Xiang, T. T., Zhou, X., and Xu, C. Y.: Impacts of climate change on the Qingjiang watershed's runoff change trend
457 in China, Stochastic Environ. Res. Risk Assess., 26, 847–858, doi:10.1007/s00477-011-0524-2, 2012.
458 Chen, J., Brissette, F. P., Poulin, A., and Leconte, R.: Overall uncertainty study of the hydrological impacts of climate change
459 for a Canadian watershed, Water Resour. Res., 47, W12509, doi:10.1029/2011WR010602, 2011.
460 Choudhury, B. J.: Evaluation of an empirical equation for annual evaporation using field observations and results from a
461 biophysical model, J. Hydrol., 216 (1–2), 99–110, 1999.
462 Christensen, N. S., Wood, A. W., Voisin, N., Lettenmaier, D. P., and Palmer, R. N.: The effects of climate change on the
463 hydrology and water resources of the Colorado River basin, Clim. Change, 62(1-3), 337–363, 2004.
464 Dooge, J. C., Bruen, M., Parmentier, B.: A simple model for estimating the sensitivity of runoff to long-term changes in
465 precipitation without a change in vegetation, Adv. Water Resour., 23 (2), 153–163, 1999.
466 Fu, B. P.: On the calculation of the evaporation from land surface, Sci. Atmos.Sin. 5 (1), 23–31, 1981. (in Chinese)
467 Fu, G., Charles, S. P., and Chiew, F. H.: A two - parameter climate elasticity of streamflow index to assess climate change
468 effects on annual streamflow, Water Resour. Res., 43, W11419, doi:10.1029/2007WR005890, 2007.
469 Garcia, M., Raes, D., Allen, R., and Herbas, C.: Dynamics of reference evapotranspiration in the Bolivian highlands
470 (Altiplano), Agricultural and forest meteorology, 125(1), 67–82, 2004.
471 Graham, L. P., Andréasson, J., and Carlsson, B.: Assessing climate change impacts on hydrology from an ensemble of
472 regional climate models, model scales and linking methods—A case study on the Lule River basin, Clim. Change, 81(S1),
473 293–307, doi:10.1007/s10584-006-9215-2, 2007.
474 Guo S., Guo, J., Zhang, J., and Chen, H.: VIC distributed hydrological model to predict climate change impact in the
475 Hanjiang basin, Sci. China Ser. E., 52, 3234–3239, 2009.
476 Harding, B. L., Wood, A. W., and Prairie, J. R.: The implications of climate change scenario selection for future streamflow
477 projection in the upper Colorado River basin, Hydrol. Earth Syst. Sci., 16, 3989–4007, 2012.
478 Harris, I., Jones, P. D., Osborna, T. J., Lister, D. H.: Updated high-resolution grids of monthly climatic observations–the
479 CRU TS3.10 Dataset, Int. J. Climatol., 34(3), 623–642, 2014.
480 Hashemi, F., Habibian, M. T.: Limitations of temperature-based methods in estimating crop evapotranspiration in arid-zone
481 agricultural projects. Agric, Forest Meteorol,, 20, 237–247, 1979.
482 IPCC: Climate Change 2013: The Physical Science Basis. Contribution of Working Group I to the Fifth Assessment Report
483 of the Intergovernmental Panel on Climate Change, edited by: Stocker, T. F., Qin, D., Plattner, G.-K., Tignor,M., Allen, S.
484 K., Boschung, J., Nauels, A., Xia, Y., Bex, V., and Midgley, P. M., Cambridge University Press, Cambridge, United
485 Kingdom and New York, NY, USA, 1535 pp, 2013.

Jung, M., and Coauthors: Recent decline in the global land evapotranspiration trend due to limited moisture supply, Nature, 467, 951–954, 2010.

Kay, A. L., Jones, R. G., and Reynard, N. S.: RCM rainfall for UK flood frequency estimation. II. Climate change results, J. Hydrol., 318, 163–172, doi:10.1016/j.jhydrol.2005.06.013, 2006.

Kay, A. L., Davies, H. N., Bell, V. A., and Jones, R. G.: Comparison of uncertainty sources for climate change impacts: flood frequency in England, Clim. Change, 92, 41–63, 2009.

Kay, A. L. and Jones, D. A.: Transient changes in flood frequency and timing in Britain under potential projections of climate change, Int. J. Climatol., 32, 489–502, 2012.

Kendall, M. G.: Rank Correlation Methods, 4th edn. Charles Grifin: London, 1975.

Li, D., Pan, M., Cong, Z., Zhang, L., and Wood, E.: Vegetation control on water and energy balance within the Budyko framework, Water Resour. Res., 49, 969–976, doi :10.1002/wrcr.20107, 2013a.

Li, F., Zhang, Y., Xu, Z., Teng, J., Liu, C., Liu, W., and Mpelasoka, F.: The impact of climate change on runoff in the southeastern Tibetan Plateau, J. Hydrol., 505, 188–201, 2013b.

Liu, L. L., Fischer, T., Jiang, T., and Luo, Y.: Comparison of uncertainties in projected flood frequency of the Zhujiang River, South China, Quat. Int., 304, 51–61, 2013.

Liu, Q., and McVicar, T. R.: Assessing climate change induced modification of Penman potential evaporation and runoff sensitivity in a large water-limited basin, J. Hydrol., 464, 352–362, 2012.

Lu, G. H., Xiao, H., Wu, Z. Y., Zhang, S. L., and Li, Y.: Assessing the impacts of future climate change on hydrology in Huang-Huai-Hai region in China using the PRECIS and VIC models. J. Hydrol. Eng., 18(9), 1077–1087, 2012.

Lute, A. C., and Abatzoglou, J. T.: Role of extreme snowfall events in interannual variability of snowfall accumulation in the western United States. Water Resour. Res. 50(4), 2874–2888, 2014.

Ma, H. A., Yang, D. W., Tan, S. K., Gao, B., Hu, Q. F.: Impact of climate variability and human activity on streamflow decrease in the Miyun Reservoir catchment, J. Hydrol., 389 (3–4), 317–324, 2010.

Malek, E.: Comparison of alternative methods for estimating ETP and evaluation of advection in the Bajah area, Iran. Agric. Forest Meteorol., 39, 185–192, 1987.

Mann, H. B.: Non-parametric tests against trend, Econometrica 13: 245–259, 1945.

McVicar, T.R., Roderick, M.L., Donohue, R.J., Li, L.T., Van Niel, T.G., Thomas, A., Grieser, J., Jhajharia, D., Himri, Y., and Mahowald, N.M.: Global review and synthesis of trends in observed terrestrial near-surface wind speeds: implications for evaporation, J. Hydrol. 416–417, 182–205, 2012.

Milly, P. C. D., and Dunne, K. A.: Macroscale water fluxes, 2. Water and energy supply control of their interannual variability, Water Resour. Res., 38(10), 1206, doi :10.1029/2001WR000760, 2002.

517 Milly, P. C., Dunne, K. A., and Vecchia, A. V.: Global pattern of trends in streamflow and water availability in a changing
518 climate, Nature, 438, 347–350, 2005.
519 Milly, P.C.D., and Dunne, K. A.: Potential Evapotranspiration and Continental Drying, Nature Climate Change 6:946–949,
520 2016.
521 Nijssen, B., Schnur, R., and Lettenmaier, D. P.: Global retrospective estimation of soil moisture using the Variable Infiltration
522 Capacity land surface model, 1980–93, J. Climate., 14, 1790–1808, 2001.
523 Oki, T., and Kanae, S.: Global hydrological cycles and world water resources, Science, 313(5790), 1068–1072, 2006.
524 Pan, M., Sahoo, A. K., Troy, T. J., Vinukollu, R. K., Sheffield, J., and Wood, E. F.: Multisource estimation of long-term
525 terrestrial water budget for major global river basins, J. Climate., 25, 3191–3206, 2012.
526 Penman, H. L.: Natural evaporation from open water, bare soil and grass. Proc. Roy. Soc. Lond. 193, 120–145, 1948.
527 Piao, S., and Coauthors: The impacts of climate change on water resources and agriculture in China, Nature, 467(7311), 43–
528 51, 2010.
529 Prudhomme, C. and Davies, H. N.: Assessing uncertainties in climate change impact analyses on river flow regimes in the
530 UK. Part 2: future climate, Clim. Change, 93, 197–222, 2009.
531 Raff, D. A., Pruitt, T., and Brekke, L. D.: A framework for assessing flood frequency based on climate projection information,
532 Hydrol. Earth Syst. Sci., 13, 2119–2136, doi:10.5194/hess-13-2119-2009, 2009.
533 Rodell, M., and Coauthors: The Global Land Data Assimilation System, Bull. Amer. Meteor. Soc., 85, 381–394, 2004.
534 Roderick, M. L., and Farquhar, G. D.: A simple framework for relating variations in runoff to variations in climatic
535 conditions and catchment properties, Water Resour. Res., 47, W00G07, doi:10.1029/2010WR009826, 2011.
536 Roderick, M. L., Sun, F., Lim, W. H., and Farquhar, G. D.: A general framework for understanding the response of the water
537 cycle to global warming over land and ocean, Hydrol. Earth Syst. Sci., 18, 1575–1589, 2014.
538 Sankarasubramanian, A., Vogel, R. M., and Limbrunner, J. F.: Climate elasticity of streamflow in the United States, Water
539 Resour. Res., 37(6), 1771–1781, 2001.
540 Schaake, J. C.: From climate to flow. In: Waggoner (Ed.), Climate Change and U.S. Water Resources, John Wiley, New York,
541 pp. 177–206, 1990.
542 Sen P. K.: Estimates of the regression coeffcient based on Kendall's tau. J. Am. Stat. Assoc., 63, 1379–1389, 1968.
543 Sheffield, J., Goteti, G., and Wood, E. F.: Development of a 50-year high-resolution global dataset of meteorological forcings
544 for land surface modeling, J. Climate., 19, 3088–3110, 2006.
545 Sheffield, J., and Wood, E. F.: Characteristics of global and regional drought, 1950–2000: Analysis of soil moisture data from
546 off-line simulation of the terrestrial hydrologic cycle, J. Geophys. Res., 112, D17115, doi: 10.1029/2006JD008288, 2007.
547 Sheffield, J., Wood, E.F., Roderick, M.L.: Little change in global drought over the past 60 years. Nature, 491, 435–438.

548 doi:10.1038/nature11575, 2012.
549 Shuttleworth, W.J.: Evaporation. In: Maidment, D.R. (Ed.), Handbook of Hydrology. McGraw-Hill, Sydney, 1993.
550 Smith, A., Bates, P., Freer, J., and Wetterhall, F.: Investigating the application of climate models in flood projection across the
551 UK, Hydrol. Process., 28, 2810–2823, doi:10.1002/hyp.9815, 2014.
552 Sperna Weiland, F. C., van Beek, L. P. H., Kwadijk, J. C. J., and Bierkens, M. F. P.: The ability of a GCM-forced
553 hydrological model to reproduce global discharge variability, Hydrol. Earth Syst. Sci., 14(8), 1595–1621, 2010.
554 Su, B., Zeng, X., Zhai, J., Wang, Y., and Li, X.: Projected precipitation and streamflow under sres and rcp emission scenarios
555 in the songhuajiang river basin, China, Quatern. Int., 380, 95–105, 2015.
556 Sun, S.L., Chen, H.S., Ju, W.M., Song, J., Zhang, H., Sun, J., Fang, Y.J.: Effects of climate change on annual streamflow
557 using climate elasticity in Poyang Lake Basin, China, Theor. Appl. Climatol. 112 (1–2), 169–183, 2013.
558 Swann, A. L., Hoffman, F. M., Koven, C. D., and Randerson, J. T.: Plant responses to increasing CO2 reduce estimates of
559 climate impacts on drought severity, Proceedings of the National Academy of Sciences, 113(36), 10019–10024, 2016.
560 Teng, J., Vaze, J., Chiew, F. H. S., Wang, B., and Perraud, J.: Estimating the Relative Uncertainties Sourced from GCMs and
561 Hydrological Models in Modeling Climate Change Impact on Runoff, J. Hydrometeor., 13, 122–139, 2012.
562 Thornthwaite, C. W.: An approach toward a rational classification of climate, Geographical Review, 38, 55–94, 1948.
563 Vano, J. A., Scott, M., Voisin, N., Stockle, C. O., Hamlet, A. F., Mickelson, K. E. B., Elsner, M. M., and Lettenmaier, D. P.:
564 Climate change impacts on water management and irrigated agriculture in the Yakima River basin, Washington, USA, Clim.
565 Change, 102(1–2), 287–317, doi:10.1007/s10584-010-9856-z, 2010.
566 Vano, J. A., et al.: Understanding uncertainties in future Colorado River streamflow, Bull. Am. Meteorol. Soc., 95, 59–78,
567 2014.
568 Vano, J. A., Nijssen, B., and Lettenmaier, D. P.: Seasonal hydrologic responses to climate change in the Pacific Northwest,
569 Water Resour. Res., 51(4), 1959–1976, 2015.
570 Wang, D., and Alimohammadi, N.: Responses of annual runoff, evaporation, and storage change to climate variability at the
571 watershed scale, Water Resour. Res., 48, W05546, doi:10.1029/2011WR011444, 2012.
572 Wang, G. Q., Zhang, J. Y., Jin, J. L., Pagano, T. C., Calow, R., Bao, Z. X., Liu, C. S., Liu, Y. L., and Yan, X. L.: Assessing
573 water resources in China using PRECIS projections and a VIC model, Hydrol. Earth Syst. Sci., 16(1), 231–240, 2012.
574 Wang, G. Q., Zhang, J. Y., Xuan, Y. Q., Liu, J. F., Jin, J. L., Bao, Z. X., He, R. M., Liu, C. S, Liu, Y. L., and Yan, X. L.:
575 Simulating the impact of climate change on runoff in a typical river catchment of the Loess Plateau, China, J. Hydrometeor.,
576 14(5), 1553–1561, 2013.
577 Watanabe, S., Kanae, S., Seto, S., Yeh, P. J. F., Hirabayashi, Y., and Oki, T.: Intercomparison of bias‐correction methods for
578 monthly temperature and precipitation simulated by multiple climate models, J. Geophys. Res., 117(D23), 2012.

579 Wu, C. H., Huang, G. R., Yu, H. J., Chen, Z. J., and Ma, J. G.: Impact of climate change on reservoir flood control in the
580 upstream area of the Beijiang River Basin, South China, J. Hydrometeor., 15, 2203–2218, doi:10.1175/JHM-D-13-0181.1,
581 2014.
582 Wu, C. H., Huang, G. R., and Yu, H. J.: Prediction of extreme floods based on CMIP5 climate models: a case study in the
583 Beijiang River basin, South China, Hydrol. Earth Syst. Sci., 19(3), 1385–1399, 2015.
584 Wu, C. H., and Huang, G. R.: Changes in heavy precipitation and floods in the upstream of the Beijiang River basin, South
585 China, Int. J. Climatol., 35(10), 2978–2992, 2015.
586 Wu, C. H., Xian, Z. Y., and Huang, G. R.: Meteorological drought in the Beijiang River basin, South China: current
587 observations and future projections, Stoch. Environ. Res. Risk Assess., 30: 1821–1834, doi:10.1007/s00477-015-1157-7,
588 2016.
589 Xiao, H., Lu, G. H., Wu, Z. Y., and Liu Z. Y.: Flood response to climate change in the Pearl River basin for the next three
590 decades, J. Hydraul. Eng., 12, 1409–1419, 2013. (in Chinese)
591 Xu, H., Taylor, R. G., and Xu, Y.: Quantifying uncertainty in the impacts of climate change on river discharge in
592 sub-catchments of the Yangtze and Yellow River Basins, China, Hydrol. Earth Syst. Sci., 15, 333–344, 2011.
593 Xu, X.Y., Yang, H.B., Yang, D.W., Ma, H.: Assessing the impacts of climate variability and human activities on annual
594 runoff in the Luan River basin, China, Hydrol. Res., 44 (5), 940–952, 2013a.
595 Xu, Y. P., Zhang, X., Ran, Q., and Tian, Y.: Impact of climate change on hydrology of upper reaches of Qiantang River Basin,
596 East China, J. Hydrol., 483, 51–60, 2013b.
597 Xu, X. Y., Yang, D. W., Yang, H. B., Lei, H. M.: Attribution analysis based on the Budyko Hypothesis for detecting the
598 dominant cause of runoff decline in Haihe basin, J. Hydrol., 510, 530–540, 2014.
599 Yan, D., Werners, S. E., Ludwig, F., and Huang, H. Q.: Hydrological response to climate change: The Pearl River, China
600 under different RCP scenarios, Journal of Hydrology: Regional Studies, 4, 228–245, 2015.
601 Yang, H., Yang, D., Lei, Z., and Sun, F.: New analytical derivation of the mean annual water - energy balance equation,
602 Water Resour. Res., 44, W03410, doi:10.1029/2007WR006135, 2008.
603 Yang, H., and Yang, D.: Derivation of climate elasticity of runoff to assess the effects of climate change on annual runoff,
604 Water Resour. Res., 47, W07526, doi:10.1029/2010WR009287, 2011.
605 Yang, H., Qi, J., Xu, X., Yang, D., and Lv, H.: The regional variation in climate elasticity and climate contribution to runoff
606 across China, J. Hydrol., 517, 607–616, 2014.
607 Zhang, L., Hickel, K., Dawes, W. R., Chiew, F. H. S., Western, A. W., and Briggs, P. R.: A rational function approach for
608 estimating mean annual evapotranspiration, Water Resour. Res., 40, W02502, doi:10.1029/2003WR002710, 2004.
609 Zhang, X., Tang, Q., Pan, M., Tang, Y.: A Long-Term Land Surface Hydrologic Fluxes and States Dataset for China, J.

Hydrometeor., 15, 2067–2084, doi: 10.1175/JHM-D-13-0170.1, 2014.

Zhang, Y., You, Q., Chen, C., and Ge, J.: Impacts of climate change on streamflows under RCP scenarios: A case study in Xin River Basin, China, Atmospheric Research, 178, 521–534, 2016.

Zheng, H., Zhang, L., Zhu, R., Liu, C., Sato, Y., and Fukushima, Y.: Responses of streamflow to climate and land surface change in the headwaters of the Yellow River Basin, Water Resour. Res., 45, W00A19, doi:10.1029/2007WR006665, 2009.

Zeng, R., Cai, X.: Climatic and terrestrial storage control on evaporation temporal variability: Analysis of river basins around the world, Geophys. Res. Lett., 43, doi:10.1002/2015GL066470, 2016.

641 **Table 1**. CMIP5 GCMs used in this study

No.	Model	Institution (Country)	Resolution
1	BCC-CSM1-1	Beijing Climate Center, China Meteorological Administration, China	1 °×1 °
2	BCC-CSM1-1-m		
3	BNU-ESM	College of Global Change and Earth System Science, Beijing Normal University, China	1 °×1 °
4	CCSM4	National Center for Atmospheric Research, USA	1 °×1 °
5	CESM1-CAM5	Community Earth System Model Contributors, USA	1 °×1 °
6	CNRM-CM5	Centre National de Recherches Météorologiques / Centre Européen de Recherche et Formation Avancée en Calcul Scientifique, France	1 °×1 °
7	CSIRO-Mk3-6-0	Commonwealth Scientific and Industrial Research Organization in collaboration with Queensland Climate Change Centre of Excellence, Australia	1 °×1 °
8	CanESM2	Canadian Centre for Climate Modelling and Analysis, Canada	1 °×1 °
9	EC-EARTH	EC-EARTH consortium	1 °×1 °
10	FGOALS-g2	LASG, Institute of Atmospheric Physics, Chinese Academy of Sciences and CESS, Tsinghua University, China	1 °×1 °
11	FIO-ESM	The First Institute of Oceanography, SOA, China	1 °×1 °
12	GFDL-CM3	NOAA Geophysical Fluid Dynamics Laboratory, USA	1 °×1 °
13	GFDL-ESM2G		
14	GFDL-ESM2M		
15	GISS-E2-H	NASA Goddard Institute for Space Studies, USA	1 °×1 °
16	GISS-E2-R		
17	HadGEM2-AO	National Institute of Meteorological Research/Korea Meteorological Administration, South Korea	1 °×1 °
18	HadGEM2-ES	Met Office Hadley Centre (additional HadGEM2-ES realizations contributed by Instituto Nacional de Pesquisas Espaciais), UK	1 °×1 °
19	IPSL-CM5A-LR	Institut Pierre-Simon Laplace, France	1 °×1 °
20	IPSL-CM5A-MR		
21	MIROC-ESM	Japan Agency for Marine-Earth Science and Technology, Atmosphere and Ocean Research Institute (The University of Tokyo), and National Institute for Environmental Studies, Japan	1 °×1 °
22	MIROC-ESM-CHEM		
23	MIROC5	Atmosphere and Ocean Research Institute (The University of Tokyo), National Institute for Environmental Studies, and Japan Agency for Marine-Earth Science and Technology, Japan	1 °×1 °
24	MPI-ESM-LR	Max-Planck-Institut für Meteorologie (Max Planck Institute for Meteorology), Germany	1 °×1 °
25	MPI-ESM-MR		
26	MRI-CGCM3	Meteorological Research Institute, Japan	1 °×1 °
27	NorESM1-M	Norwegian Climate Centre, Norway	1 °×1 °
28	NorESM1-ME		

642

643

Table 2. The estimations of *P* elasticity, *PET* elasticity, and catchment properties elasticity of *R* in the 14 river basins of China based on Equations (2) and (3). The basin number is consistent with that given in Figure 1. The numbers in the parentheses indicate the 1960–2008 mean aridity index.

Basin No.	ε_P		ε_{PET}		ε_n or ε_ω	
	Eq.(2)	Eq.(3)	Eq.(2)	Eq.(3)	Eq.(2)	Eq.(3)
1 (0.52)	1.64	1.65	-0.64	-0.65	-0.24	-0.33
2 (0.64)	1.63	1.64	-0.62	-0.63	-0.41	-0.61
3 (0.81)	1.55	1.56	-0.55	-0.55	-0.57	-0.93
4 (1.19)	1.40	1.39	-0.40	-0.39	-0.73	-1.44
5 (1.19)	2.09	2.08	-1.08	-1.07	-1.03	-1.47
6 (1.43)	2.06	2.04	-1.05	-1.02	-1.25	-1.83
7 (1.71)	1.92	1.88	-0.91	-0.87	-1.35	-2.10
8 (2.14)	2.28	2.21	-1.29	-1.22	-1.89	-2.70
9 (2.38)	1.78	1.72	-0.79	-0.73	-1.53	-2.54
10 (4.41)	2.23	2.11	-1.22	-1.10	-2.78	-4.16
11 (4.70)	1.81	1.72	-0.82	-0.72	-2.17	-3.67
12 (6.68)	1.72	1.62	-0.73	-0.63	-2.28	-4.08
13 (8.09)	1.66	1.56	-0.65	-0.55	-2.26	-4.27
14 (8.63)	1.63	1.53	-0.64	-0.54	-2.26	-4.30

Table 3. The contributions of *P*, *PET*, and climate (i.e. *P& PET*) to *R* in the 14 basins of China for the period 1960–2008. The basin number is consistent with that given in Figure 1. The numbers in the parentheses indicate the 1960–2008 mean aridity index.

Basin No.	*P* (%/a)	*PET* (%/a)	*P&PET* (%/a)
1 (0.52)	0.19	-0.13	0.06
2 (0.64)	-0.03	-0.09	-0.12
3 (0.81)	-0.07	-0.07	-0.14
4 (1.19)	0.14	-0.01	0.13
5 (1.19)	-0.18	-0.27	-0.45
6 (1.43)	-0.35	-0.31	-0.66
7 (1.71)	-0.57	-0.34	-0.91
8 (2.14)	-0.74	-0.38	-1.12
9 (2.38)	-0.38	-0.04	-0.42
10 (4.41)	-0.40	-0.26	-0.66
11 (4.70)	0.99	0.01	1.00
12 (6.68)	0.43	-0.01	0.42
13 (8.09)	0.84	-0.02	0.82
14 (8.63)	0.11	0.08	0.19

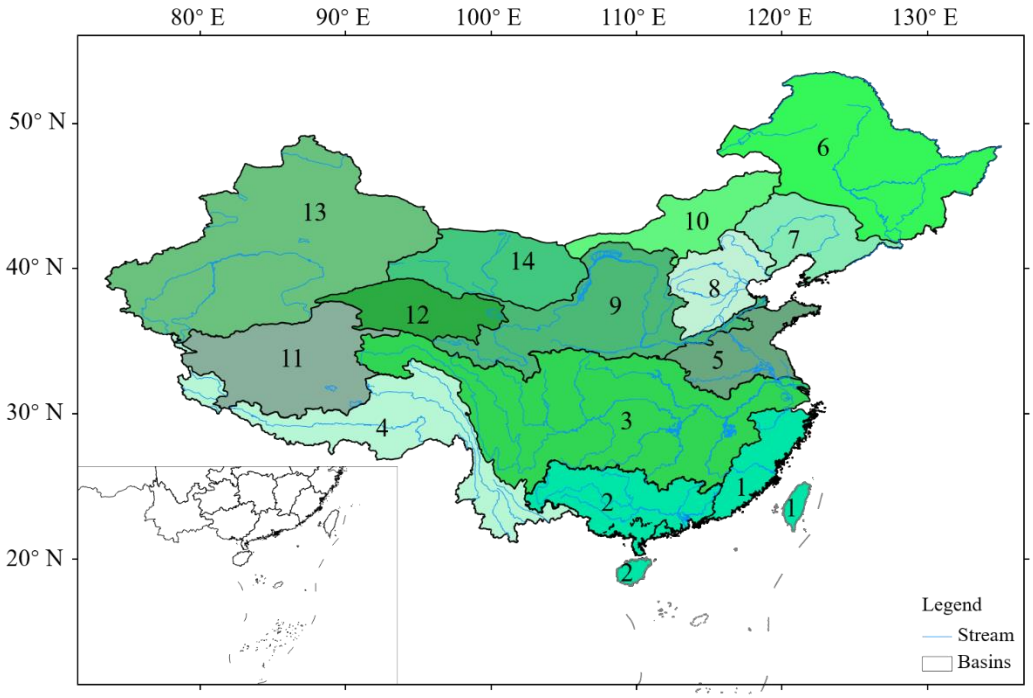

Figure 1. Location of the main river basins in China. The numbers denote the river basins with increasing aridity index: 1, Southeast Drainage (0.52); 2, Pearl River (0.64); 3, Yangtze River (0.81); 4, Southwest Drainage (1.19); 5, Huaihe River (1.19); 6, Heilongjiang River (1.43); 7, Liaohe River (1.71); 8, Haihe River (2.14); 9, Yellow River (2.38); 10, Inner Mongolia River (4.41); 11, Qiangtang River (4.70); 12, Qinghai River (6.68); 13, Xinjiang River (8.09), 14, Hexi River (8.63). The numbers in the parentheses indicate the 1960–2008 mean aridity index.

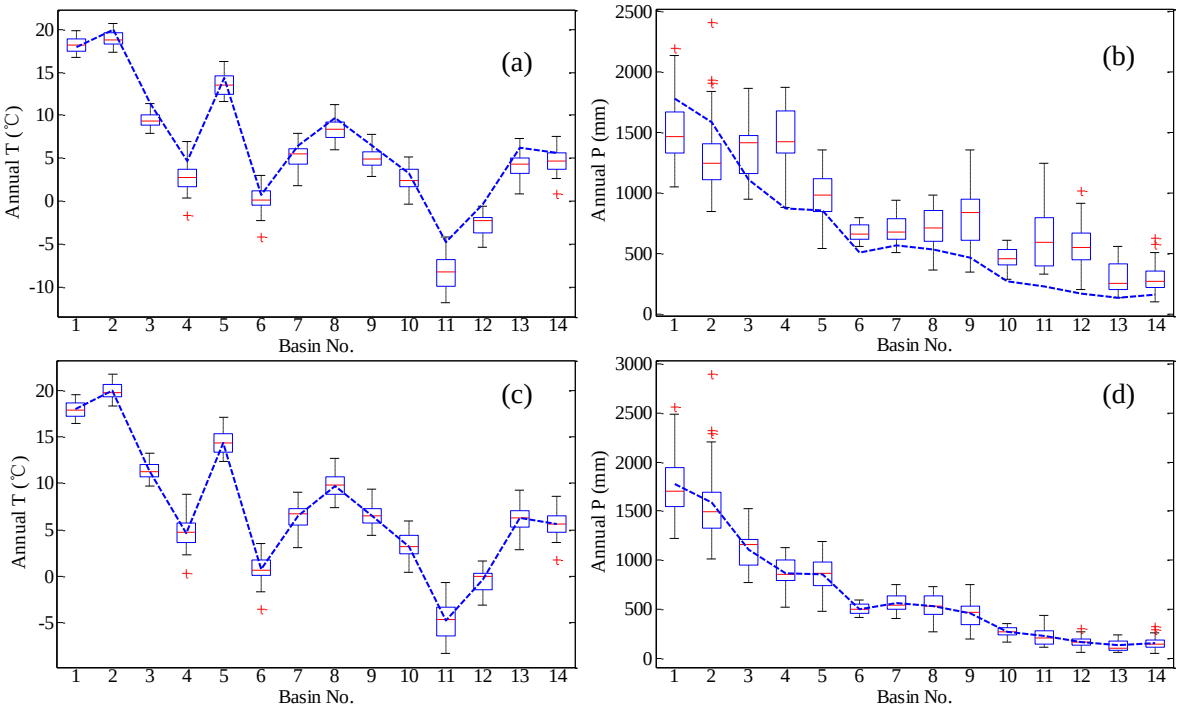

Figure 2. Box plots of the simulation results of (a) mean annual *T* and (b) mean annual *P* and the bias correction results of (c) mean annual *T* and (d) mean annual *P* from 28 GCMs for the period 1971–2000 in the 14 river basins. The boxes denote the interquartile model spread (range between the 25th and 75th quantiles), with the horizontal line indicating the ensemble median and the whiskers showing the extreme range of the 28 CMIP5 model simulations. The blue dotted lines denote the observed results of mean annual *T* and mean annual *P* for the period 1971–2000. The basin number is consistent with that given in Figure 1.

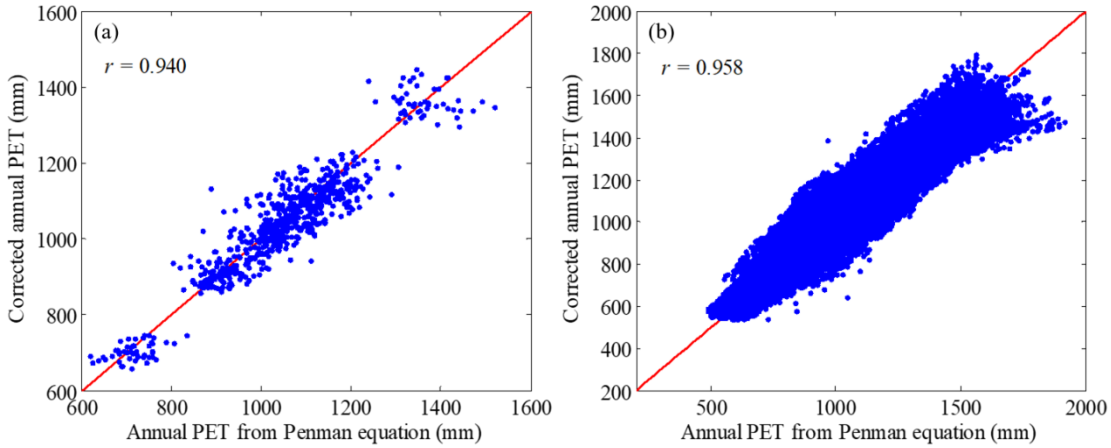

686

687 **Figure 3.** Comparison of annual *PET* calculated from the Penman method and the Thornthwaite method
688 corrected by Equation (1) during the period 1960–2008 for (a) the 14 river basins and (b) all 0.5° grid
689 points over China.

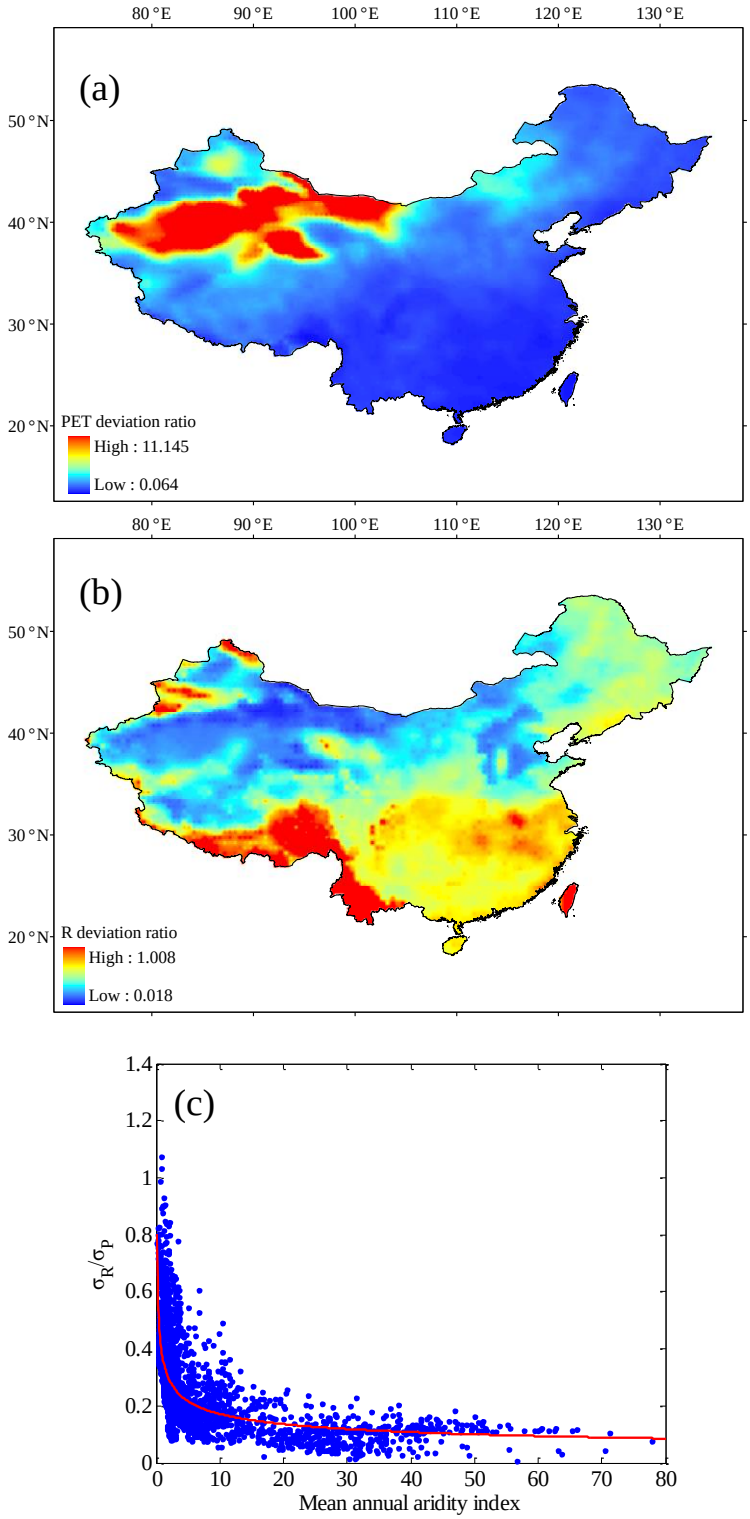

690

691 **Figure 4.** Spatial distributions of (a) *PET* deviation ratio and (b) *R* deviation ratio and (c) the

692 relationship between *R* deviation ratio and mean annual aridity index ($\bar{\phi}$) for all 0.5^{o} grid points in

693 China.

694

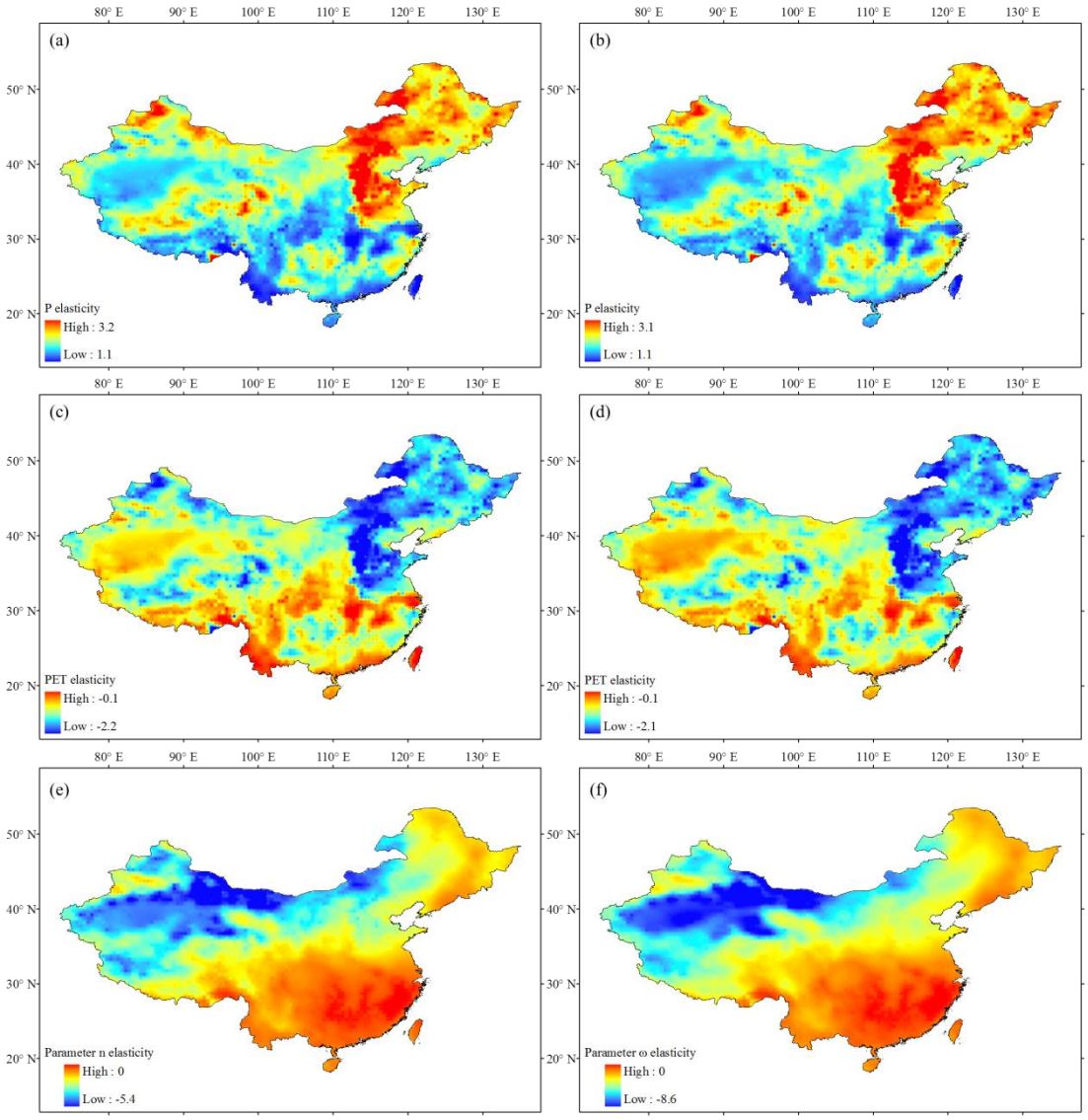

Figure 5. Spatial distributions of the *P* elasticity of *R* across China from (a) Equation (2) and (b) Equation (3). Spatial distributions of the *PET* elasticity of *R* across China from (c) Equation (2) and (d) Equation (3). Spatial distributions of the parameter elasticity of *R* across China from (e) Equation (2) and (f) Equation (3).

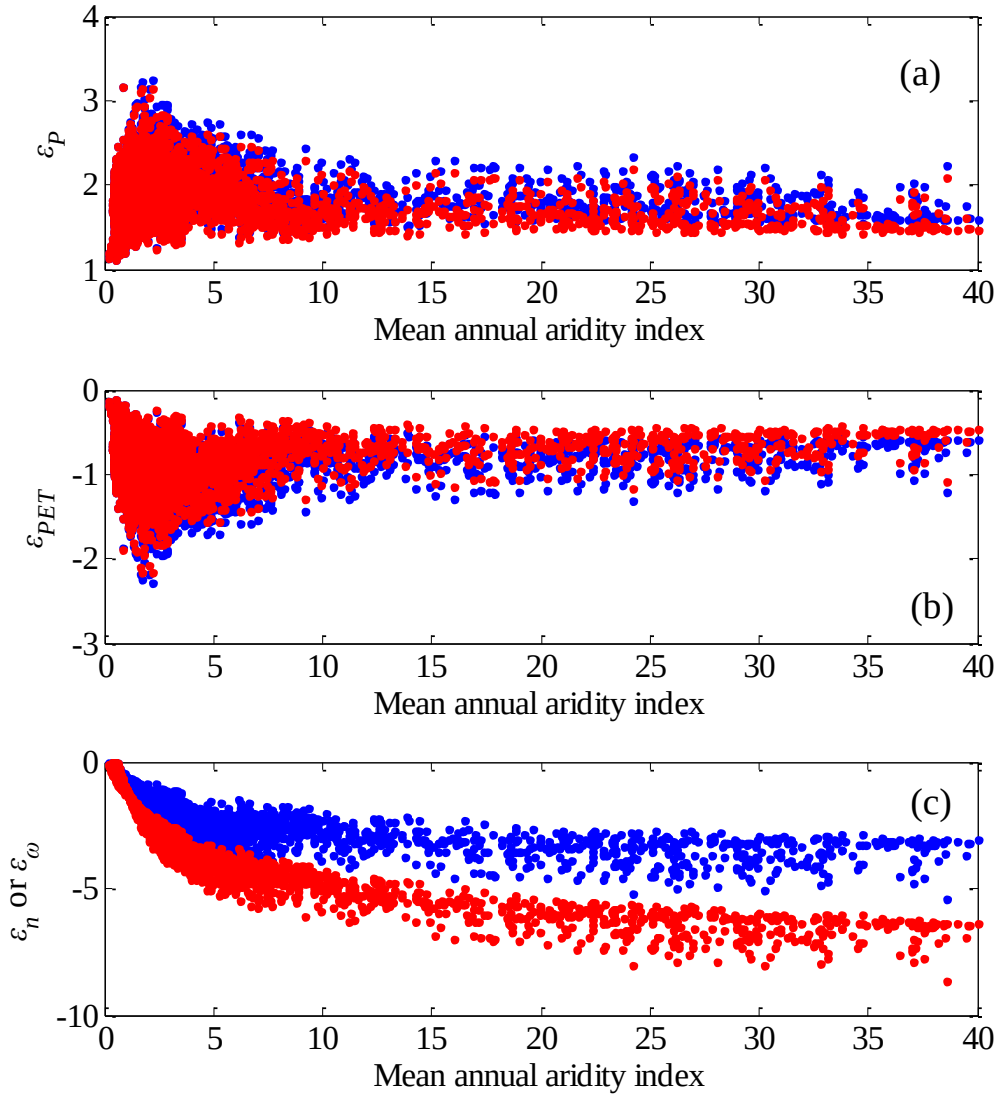

Figure 6. The relationship between mean annual aridity index and (a) *P* elasticity, (b) *PET* elasticity, and (c) parameter elasticity. The blue points represent the case of Equation (2), and the red points represent the case of Equation (3).

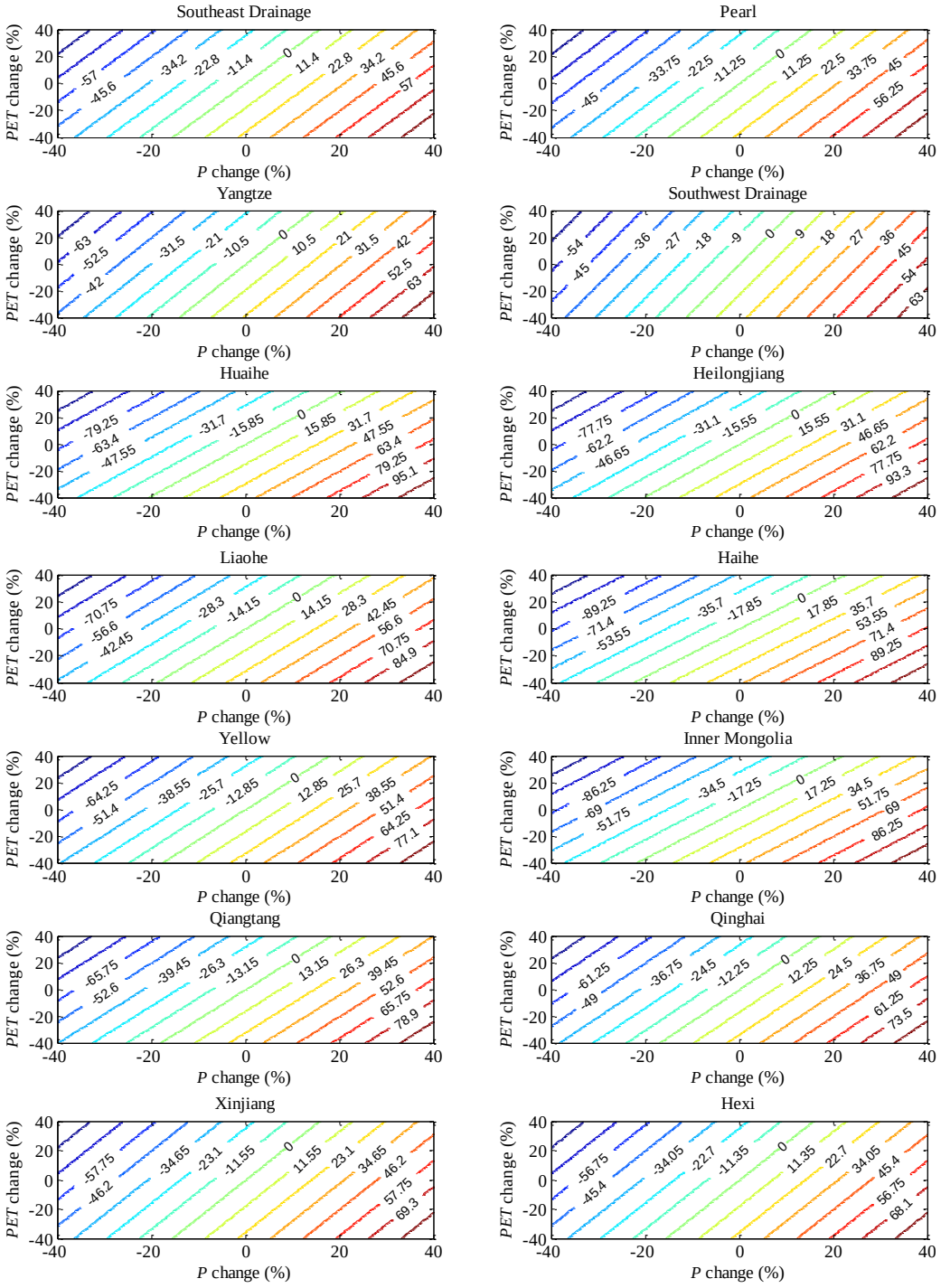

714

715 **Figure 7**. Contour plot of percentage *R* change due to the changes in *P* and *PET* for the 14 river basins.

716 The *P* elasticity and *PET* elasticity of *R* are estimated based on Equation (2).

717

718

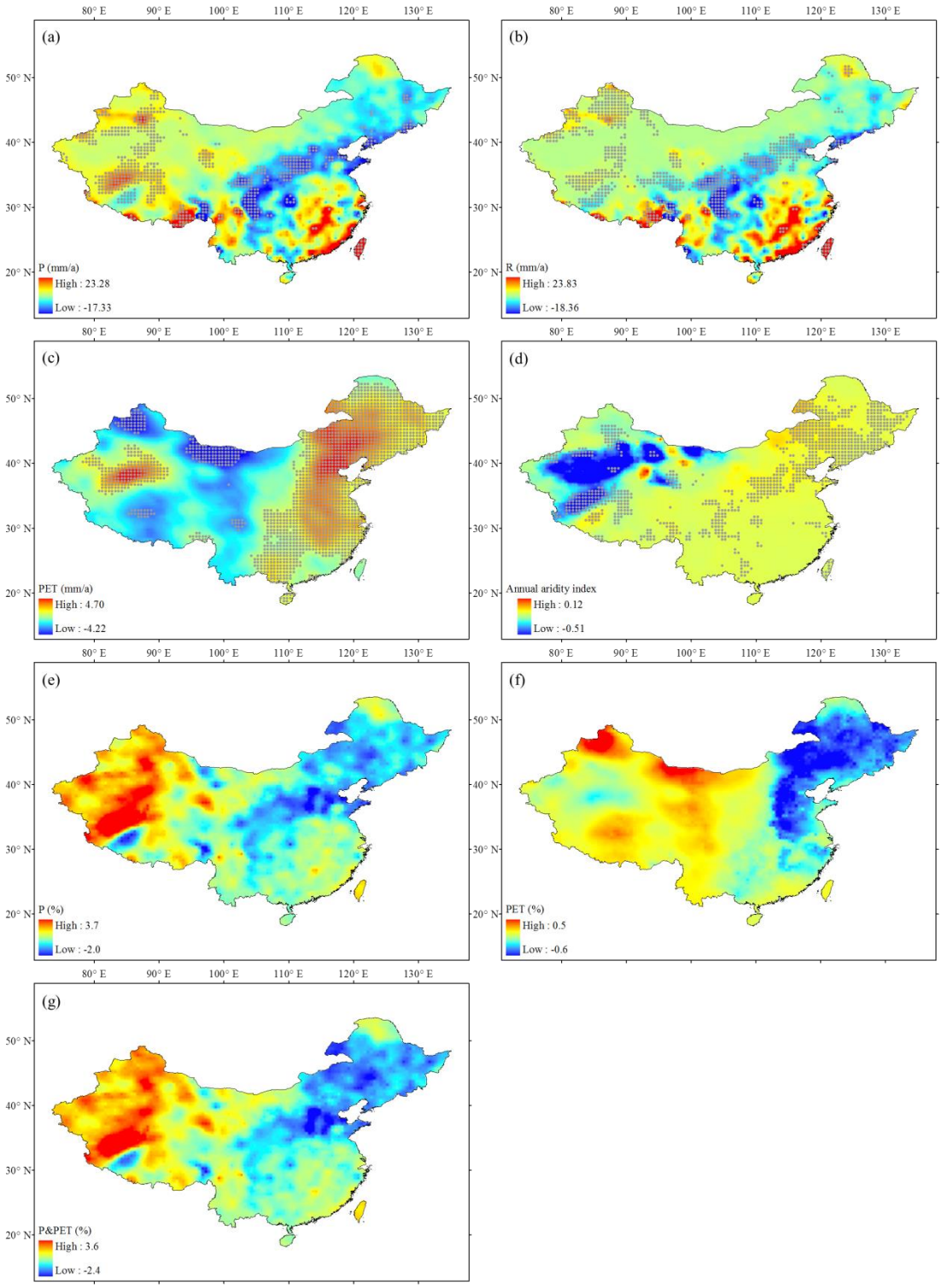

719

720 **Figure 8.** Trend magnitudes in annual time series of (a) *P*, (b) *R*, (c) *PET*, and (d) aridity index for the
721 period 1960–2008 and spatial distributions of the contributions (unit: % yr^{-1}) of (e) *P*, (f) *PET*, and (g)
722 climate (i.e. *P& PET*) to *R* in China for the period 1960–2008. The trend magnitudes are estimated by
723 the Sen's method. Grey dots are shown as statistically significant positive/negative trends ($p < 0.05$).

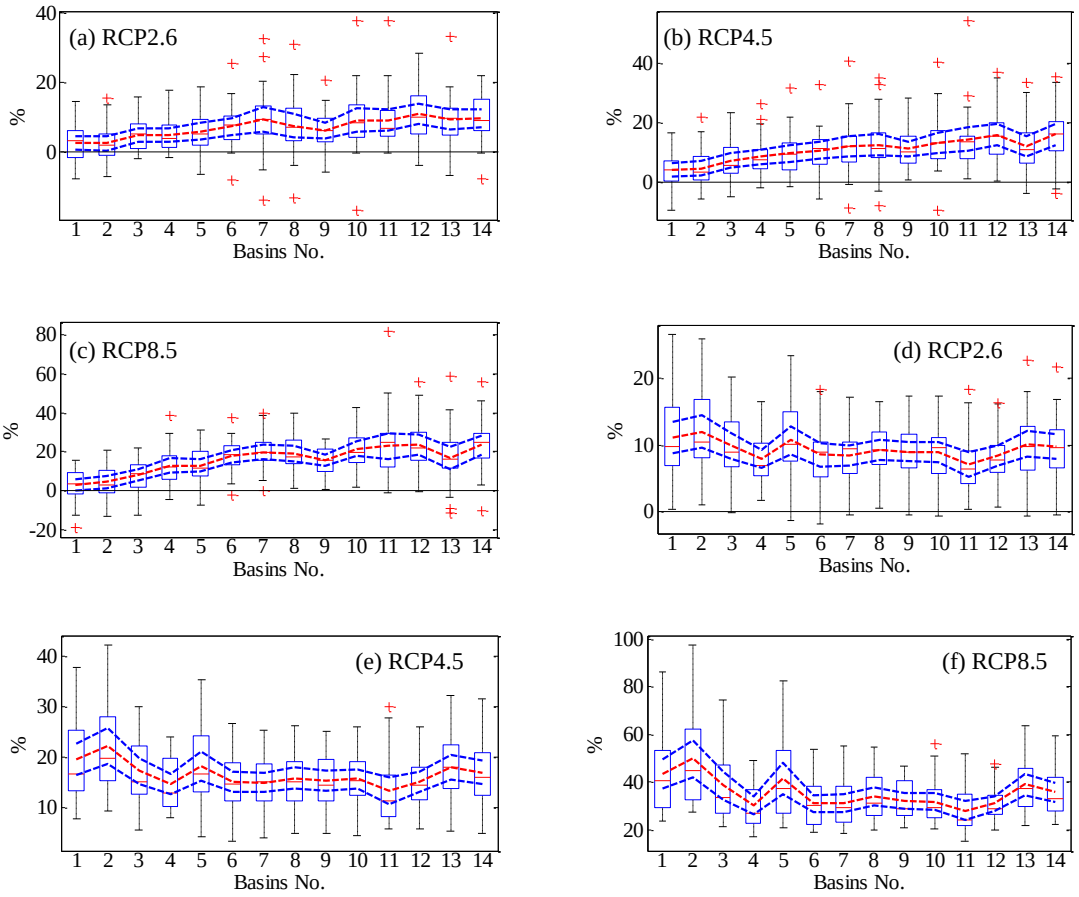

Figure 9. Box plots of relative change (%) in mean annual *P* under (a) RCP2.6, (b) RCP4.5, and (c) RCP8.5 scenarios and in mean annual *PET* under (d) RCP2.6, (e) RCP4.5, and (f) RCP8.5 scenarios calculated from 28 CMIP5 models in 14 basins for the period 2071–2100 (relative to the baseline 1971–2000). The boxes denote the interquartile model spread (range between the 25th and 75th quantiles), with the horizontal line indicating the ensemble median and the whiskers showing the extreme range of the 28 CMIP5 model simulations. Red dotted lines denote the average values of the multi-model ensemble. Blue dotted lines denote the 95 % significance levels range of the average values of the multi-model ensemble. The basin number is consistent with that given in Figure 1.

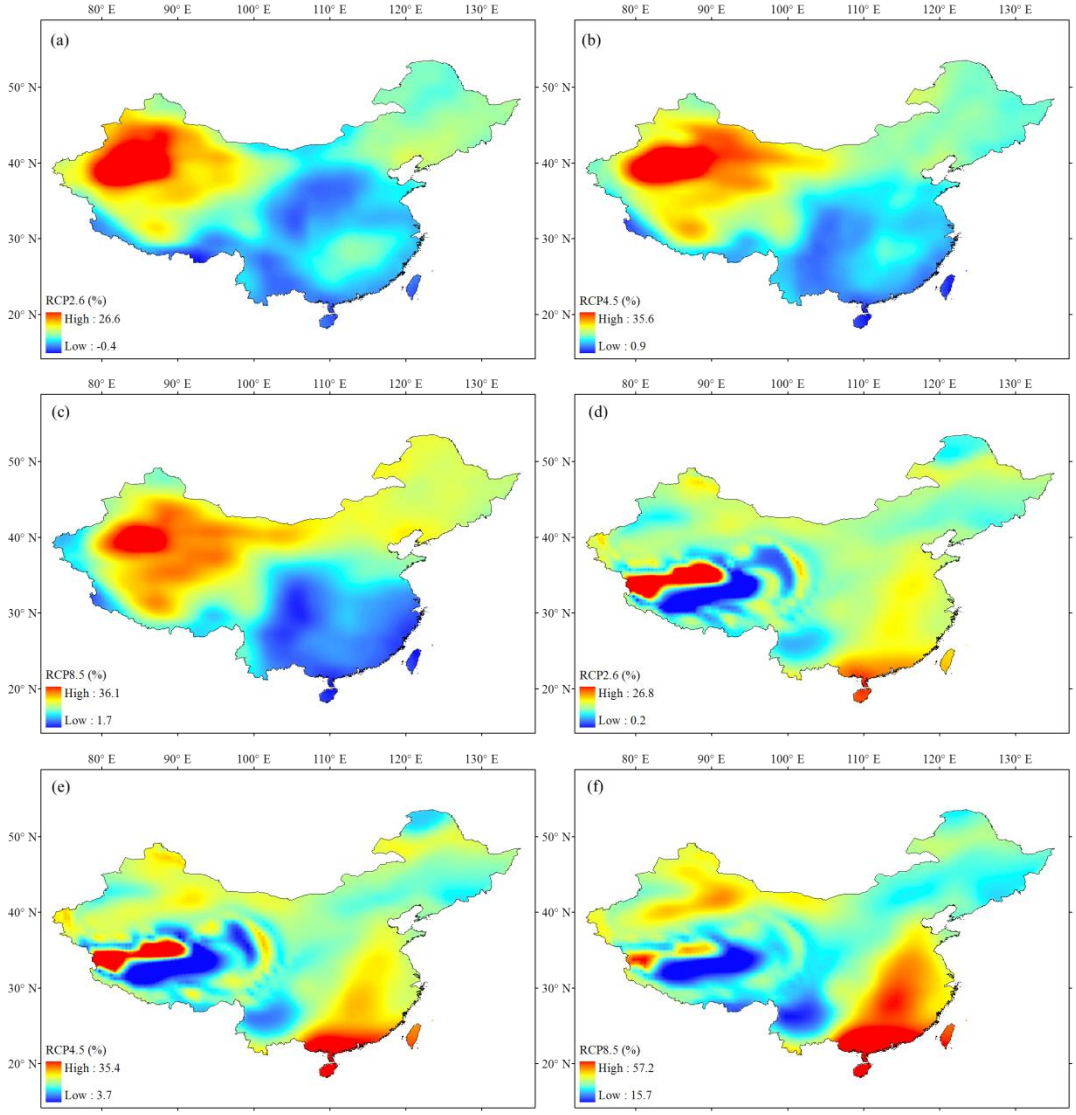

Figure 10. The CMIP5 multi-model ensemble median relative change (%) in mean annual *P* under (a) RCP2.6, (b) RCP4.5, and (c) RCP8.5 scenarios and in mean annual *PET* under (d) RCP2.6, (e) RCP4.5, and (f) RCP8.5 scenarios in China for the period 2071–2100 (relative to the baseline 1971–2000).

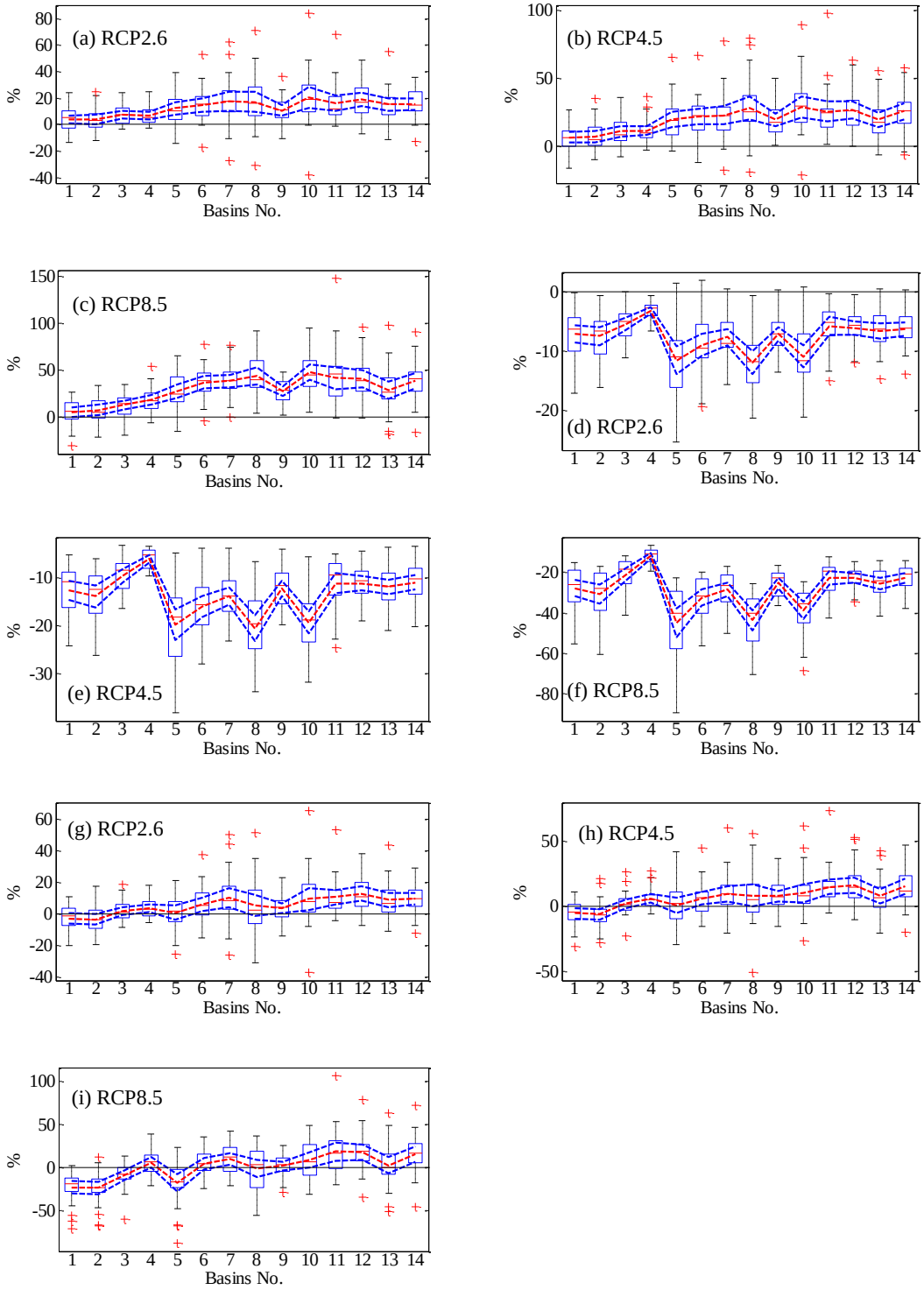

746

747 **Figure 11**. Box plots of relative change (%) in the contributions of annual *P* to *R* under (a) RCP2.6, (b)
748 RCP4.5, and (c) RCP8.5 scenarios, in the contributions of annual *PET* to *R* under (d) RCP2.6, (e)
749 RCP4.5, and (f) RCP8.5 scenarios, and in the contributions of climate to *R* under (g) RCP2.6, (h)
750 RCP4.5, and (i) RCP8.5 scenarios calculated from 28 CMIP5 models in 14 basins for the period 2071–
751 2100 (relative to the baseline 1971–2000). The boxes denote the interquartile model spread (range
752 between the 25th and 75th quantiles) with the horizontal line indicating the ensemble median and the
753 whiskers showing the extreme range of the 28 CMIP5 model simulations. Red dotted lines denote the

average values of the multi-model ensemble. Blue dotted lines denote the 95% significance levels range of the average values of the multi-model ensemble. The basin number is consistent with that given in Figure 1.

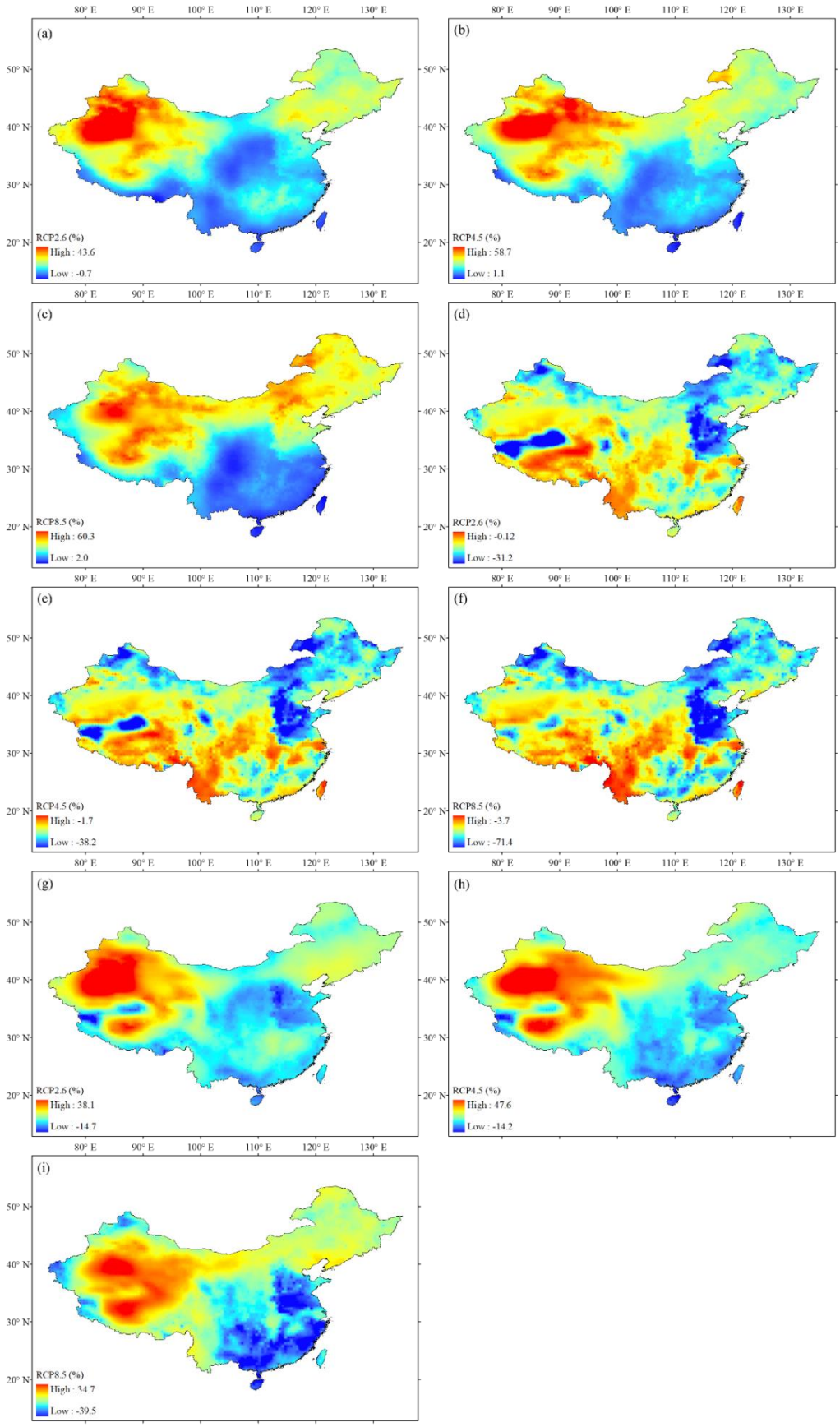

779

780 **Figure 12**. The CMIP5 multi-model ensemble median relative change (%) in the contributions of

781 annual *P* to *R* under (a) RCP2.6, (b) RCP4.5, and (c) RCP8.5 scenarios, in the contributions of annual

782 *PET* to *R* under (d) RCP2.6, (e) RCP4.5, and (f) RCP8.5 scenarios, and in the contributions of climate

to *R* under (g) RCP2.6, (h) RCP4.5, and (i) RCP8.5 scenarios in China for the period 2071–2100 (relative to the baseline 1971–2000).

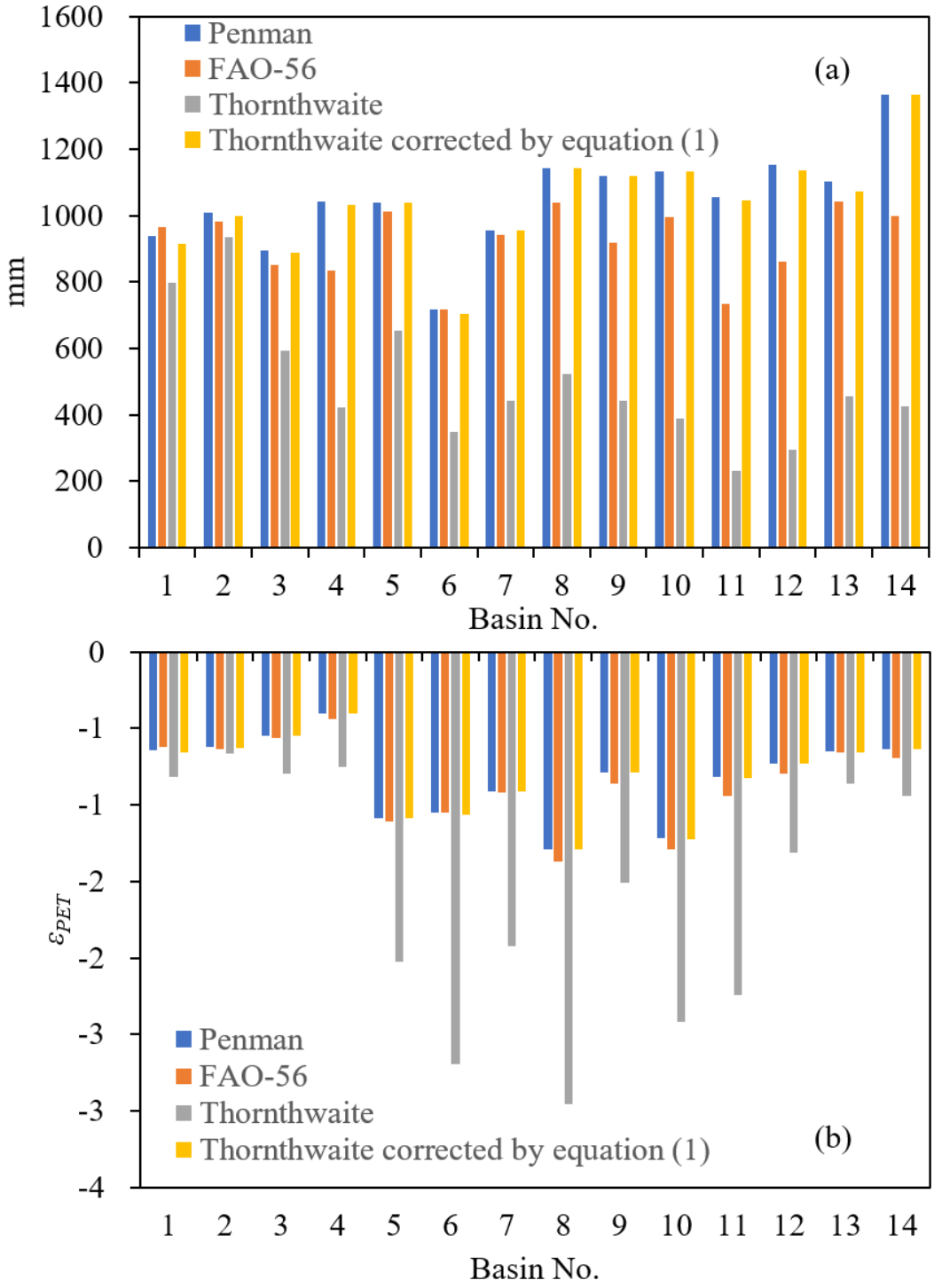

Figure 13. (a) Mean annual *PET* calculated from the four methods for the 14 river basins of China during the period 1960–2008. (b) *PET* elasticity calculated from Equation (2) based on the four *PET* data for the 14 river basins of China during the period 1960–2008. The basin number is consistent with that given in Figure 1.

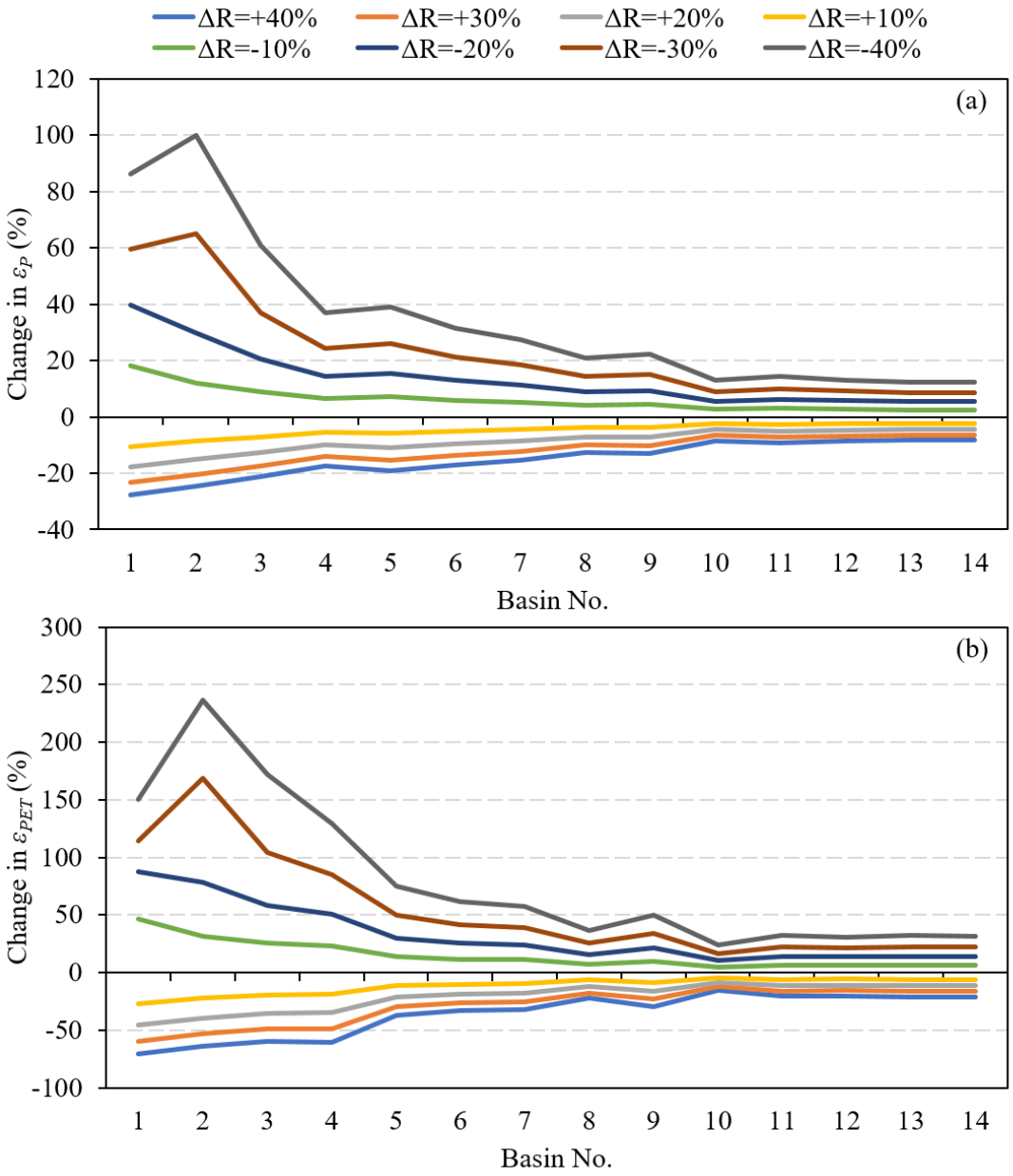

814

815 **Figure 14**. Comparison of changes in (a) *P* elasticity and (b) *PET* elasticity in response to changes in *R*

816 for the 14 river basins of China. The basin number is consistent with that given in Figure 1.

817